2022

THERMOMECHANICAL EVOLUTION OF A MAGMATIC SYSTEM DURING A CALDERA CYCLE: OKATAINA VOLCANIC CENTER, NEW ZEALAND

Jacob Bonessi
Michigan Technological University, jmboness@mtu.edu

THERMOMECHANICAL EVOLUTION OF A MAGMATIC SYSTEM DURING A CALDERA CYCLE: OKATAINA VOLCANIC CENTER, NEW ZEALAND

By

Jacob M. Bonessi

A THESIS

Submitted in partial fulfillment of the requirements for the degree of

MASTER OF SCIENCE

In Geology

MICHIGAN TECHNOLOGICAL UNIVERSITY

2022

This thesis has been approved in partial fulfillment of the requirements for the Degree of MASTER OF SCIENCE in Geology.

Department of Geological and Mining Engineering and Sciences

Thesis Advisor: *Dr. Chad Deering*

Committee Member: *Dr. Greg Waite.*

Committee Member: *Dr. Adam Kent*

Department Chair: *Dr. Aleksey Smirnov*

Table of Contents

List of Figures

List of Tables

Acknowledgements

I would like to thank Dr. Chad Deering for the work that he does to provide opportunities for not only me, but also to his clade of students for the duration of their research projects. The GMES department at MTU is also owed a thank you for their part in cultivating student opportunities. Thanks to the efforts of Dr. Deering and MTU GMES, my experience during the completion of the degree has provided me with a rich experience that was undoubtedly well worth the effort.

Thank you, Dr. Greg Waite, for agreeing to be on my committee in short notice.

I would also like to thank several people at Oregon State University that helped me along during my data collection marathon. Dr. Adam Kent, thanks for being a part of the project and getting me in touch with Dr. Frank Tepley and Dr. Chris Russo, who both helped immensely during my time in the labs at OSU.

Abstract

Caldera forming eruptions represent some of the largest simultaneous releases of mass and energy on the planet and pose a looming risk on a global scale. The study of the underlying magmatic systems is integral in understanding what leads to these large eruptions. This approach pairs a suite of major and trace element profiles from plagioclase with a grain texture classification and statistical analysis using Polytopic Vector Analysis (PVA) as proxies to explore potential changes in the thermomechanical state of the magmatic system at Okataina Volcanic Complex (OVC), New Zealand through its most recent caldera cycle. Results indicate systematic changes in plagioclase chemistry and textures that are highlighted by: 1) pre-caldera crystals that are compositionally evolved yet primarily fed by a mafic chemical end-member, 2) syn-caldera crystals that are compositionally heterogenous yet texturally restricted, and 3) post-caldera crystals that are initially texturally broad and least evolved but migrate towards pre/post compositions and textures by the end of the analyzed samples. Paired with the contributions of the four distinct geochemical end-members generated using PVA, it is suggested that OVC was primarily in a "cold storage" state during the pre- and post-caldera timeframe, while a "warm" storage scenario best describes the state of the system during the building of the syn-caldera eruptions.

1 Introduction

Volcanic systems that have produced caldera forming eruptions are a topic of continued interest in geologic investigations (e.g., Bailey et al., 1976; Cole et al., 2010; Sawyer et al., 1994; Wilson et al., 1984). Caldera forming eruptions, although rare, have the potential to wreak havoc at a scale not seen in the modern era of human history. Due to the inherent risk posed to local areas by these catastrophic eruptions, the understanding of these systems is of paramount importance.

The Taupo Volcanic Zone (TVZ), located on the North Island of New Zealand, is the one of the most active Quaternary silicic system in the world and is characterized by small scale rhyolitic volcanism punctuated by large scale caldera forming eruptions (Houghton et al., 1995). Due to the longevity and recent nature of the volcanic activity at the TVZ, the extensive exposure of volcanic stratigraphy provides a unique opportunity to study the chronologic evolution a magmatic complex that has generated over 30 caldera forming eruptions since its inception 1.6 Ma (Wilson et al., 1995).

Zoned plagioclase crystals are ubiquitous in the entire range of volcanic rocks generated in the TVZ. Due to the prevalence of plagioclase in the rocks produced here, it serves as a useful metric when probing the conditions of the magmatic system during the residence of the crystals. Magmatic plagioclase, although stable in a broad range of temperatures and pressures, can take many forms as it is sensitive to changes in environmental parameters in the melt (e.g., Nixon & Pearce, 1987; Smith et al., 2010; Tepley et al., 1999). The history of each plagioclase crystal is recorded as growth occurs outwardly in layers during favorable environmental conditions. The mineral can also record periods of dissolution, or erosion, during unfavorable conditions. The compositions of the growth layers, or zones, primarily depends on the temperature and composition of the melt. Investigations of the textural characteristics and chemical compositions of zonation in plagioclase have been widely used to gain insight on conditions of the magmatic system from which the crystals were produced and often invoke processes such as magma mixing, fractional crystallization, and convective stirring to explain the chemical and optical variations in

zoning patterns (e.g.: Ginibre, Wörner, et al., 2002; Nixon & Pearce, 1987; Pearce et al., 1987; Shane, 2015).

Although the paring of qualitative textural analysis with geochemical analysis often provides sufficient evidence to interpret magmatic conditions, multivariate statistical methods are occasionally summoned to aid in highlighting fine details in geochemical datasets (e.g.: Brandmeier & Wörner, 2016; Pitcher & Kent, 2019; Tefend et al., 2007; Vogel et al., 2008). A select multivariate method, Polytopic Vector Analysis (PVA), not only attempts to discern the number of end-members (EM) in a magmatic system, but also the composition of each EM and the proportion of each in the individual dataset entries (Deering et al., 2008; Szymanski et al., 2013; Vogel et al., 2008). Although this method has traditionally been used with whole rock datasets, several studies applied PVA in mineral studies (e.g.: Apatite; Lisowiec et al., 2015, Plagioclase; Słaby et al., 2017)

In this study, we combine textural, geochemical, and statistical analysis of plagioclase from eruptions that bracket the most recent caldera forming eruption derived from the Okataina Volcanic Center (OVC) in the TVZ. This approach is used to demonstrate the fundamental changes in the magmatic system at a volcanic center through an entire caldera cycle, i.e. pre, syn and post-caldera. The novel approach of using PVA on magmatic plagioclase from a large silicic volcanic center supports evidence of systematic changes in of the magmatic system through time.

2 Geologic setting

Okataina Volcanic Center is a caldera complex located in the North Island of New Zealand. It is one of eight volcanic centers that occurs in the Taupo Volcanic Zone, a NW trending rifting volcanic arc (Figure 2.1). The volcanic arc is influenced by the oblique convergence of the oceanic Pacific Plate with the continental Australian Plate. The rate of subduction decreases towards the transition to a transform boundary in the South Island (Clark et al., 2019). The asymmetric ~20° convergence along the NE – SW trending Hikurangi subduction margin generates rifting between the eastern limb and main body of the North Island. The resulting thinning of the crust from active rifting has been accompanied by upwellings of subduction derived fluids which promote significant partial melting of the mantle wedge, which feeds the upper crustal magmatic systems in the TVZ (Deering et al., 2008; Rooney & Deering, 2014).

The culmination of crustal thinning and active magmatism has produced extensive volcanic activity in the TVZ. The southern and northern extents (Mt. Ruapehu and White Island respectively) have predominantly intermediate composition volcanism, while rhyolite production has been focused in the central TVZ. Rhyolite production has varied temporally and spatially throughout the history of the TVZ (Wilson et al., 1995).

The Okataina segment of the TVZ rift is characterized by a high degree of extension and voluminous volcanic activity (Spinks et al., 2005). The volcanic activity at this caldera complex is characterized by intermittent infilling eruptions of small to moderate volume (5 – 15km^3). Periodically, large (>100 km^3) rhyolitic eruptions have occurred and drastically reshaped the structure and geography of the OVC. The complex is currently subdivided into the northern Haroharo Volcanic Complex (HVC) and southern Tarawera Volcanic Complex (TVC).

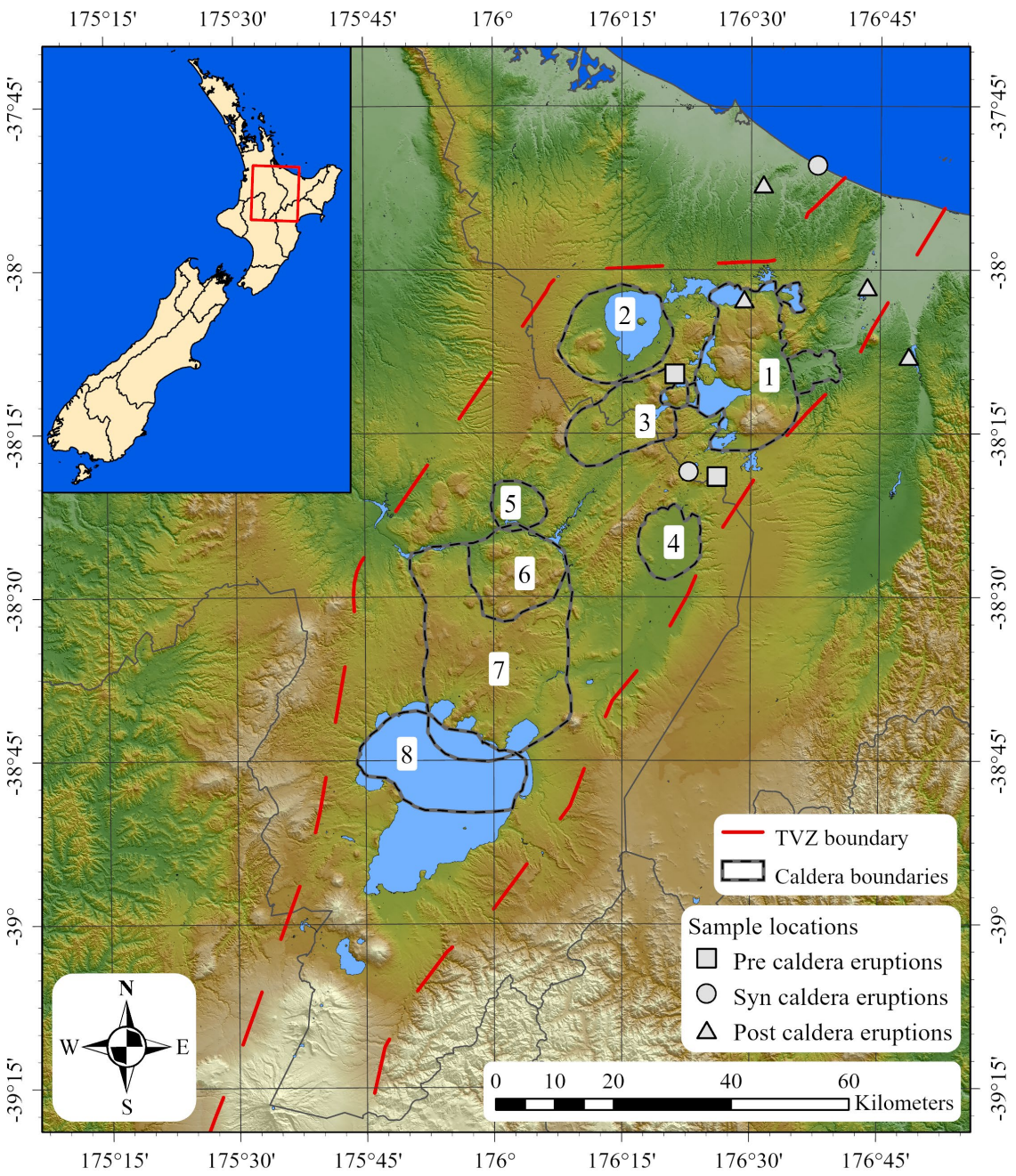

Figure 2.1: Map of the modern TVZ and associated historic caldera complexes modified from (Cole & Spinks, 2009; Nairn, 2002; Spinks et al., 2005). Caldera names (1: Okataina, 2: Rotorua, 3: Kapenga, 4: Reporoa, 5: Ohakuri, 6. Moroa, 7. Whakamaru, 8. Taupo). Distal and proximal deposits from eruptions sourced from OVC magmatism were sampled.

2.1 OVC eruptive history

The volcanic evolution at Okataina has been reported in previous studies (see Cole et al., 2010 for eruptive history) and a simplified version is reported here (Table 2.1). Volcanic activity in the OVC may have commenced around 650 ka based on distal tephra that contains cummingtonite, which is a rare mineral assemblage only found in OVC rhyolites (Ewart, 1971; Manning, 1996). Since the onset of volcanism in the OVC, intermittent activity has been punctuated by caldera forming eruptions. The OVC has had three significant caldera collapse events during its ~650 ka history: 1) Quartz-biotite (~550 ka), 2) Matahina (~325 ka), and 3) Rotoiti (~45 ka) (Bailey & Carr, 1994; Danišík et al., 2012; Nairn, 2002). During the interim between caldera forming eruptions, smaller and more frequent events occurred within and on the flanks of the OVC caldera complex.

During the previous 350 ka, Okataina has erupted over 350 km^3 of magma (Cole et al., 2010; V. C. Smith et al., 2005). Following the Matahina event, the preserved temporal distribution of OVC eruptions is highly skewed, with 18 of 21 eruptions occurring between 325ka – 240ka. The Onuku and Pokopoko Pyroclastics occurred during this active post-caldera volcanism. Onuku eruptions produced multiple pyroclastic and non-welded flow deposits that occur to the south and east of OVC and form contacts between the older Matahina Ignimbrite and younger 240 ka Kaingaroa Ignimbrite (Reporoa Caldera source). At least six individual eruptions, separated by paleosols, have been assigned this pyroclastic subgroup. The pyroclastic and fall deposits from the Pokopoko eruptions occur at the western margin of the OVC and are overlain by the Mamaku Ignimbrite (240 ka; Rotorua Caldera source) (Nairn, 2002). Vents for these eruptions are poorly constrained, as with all OVC sourced eruptions that preceded the Rotoiti event.

A perceived dearth of activity between 240 – 45ka was interrupted by the Rotoiti event, the most recent caldera forming event at Okataina. Evidence from mingled pumice and mineralogy and geochemical signatures suggest a link between the eruptive products of the late stage Rotoiti event and the Earthquake Flat event. The Earthquake Flat eruption occurred southwest of the Rotoiti eruptions along a series of NW trending vents shortly

after the continuous Rotoiti eruptive phase that produced > 100 km^3 of magmatic equivalent (Molloy et al., 2008). Earthquake Flat was an order of magnitude smaller than the Rotoiti event, and produced ~10 km^3 (Nairn, 2002).

Intracaldera volcanism defined the activity at Okataina following the caldera collapse of the Rotoiti event. The Mangaone Subgroup, which lies between the Rotoiti deposits and the Taupo sourced Oruanui deposit (26.5ka), is comprised of at least twelve individual Plinian fall deposits (Unit A – Unit L). The oldest Mangaone eruptive products following Rotoiti are characterized by low SiO_2 rhyodacites. Eruptions during the younger Mangaone sequence are characterized by a return to high SiO_2 rhyolites (Smith et al., 2002) The locations of Mangaone vents are not well constrained due to limited exposure, but most eruptions likely occurred west of the Puhipuhi embayment or along a N-S trend between the HVC and TVC (Figure 2.2; Jurado-chichay & Walker, 2000).

Following the 26.5ka Oruanui episode from TVC, intracaldera eruptions continued to define the activity in OVC. Eruptions within the OVC during the last 26.5ka consist of at least nine separate rhyolitic eruptions and several accompanying minor basaltic eruptions. These eruptions occurred in the northern Haroharo and southern Tarawera linear vent zones. These linear vent zones, which both trend NE, are roughly parallel to the predominant structural fabric of the TVZ (Nairn, 1989). Of the >80 km^3 of magma that was erupted during this period, the Haroharo vents have produced the volumetric majority and more frequent eruptions. The most recent eruption from OVC came from Tarawera however. The 21ka TeRere eruptive episode is the oldest event that can be attributed to the post 26.5ka sequence of rhyolites from OVC and is represented by ash fall and lava flows that were produced along a long stretch of the Haraharo vent zone (Figure 2.2). Eruptions after the TeRere episode occurred at 1.5-5 ka intervals and occurred from multiple vents along the respective linear vents zones (Smith et al., 2005). The Kaharoa eruption (age: 665 ± 15 BP) the most recent rhyolitic eruption at OVC (Lowe et al., 1998). Although basaltic eruptions represent a volumetric minority in the OVC and TVZ, the historic Tarawera sourced eruption in 1886 AD was induced by a series of basaltic dike intrusions

and subsequent eruptions from a 17 km long rift that formed during the event (Nairn & Cole, 1981).

Table 2.1 Simplified stratigraphy of OVC eruptive products. Ages: (1: Danišík et al., 2020; 2: Lowe et al., 1998) Volumes (Cole et al., 2014; Manning, 1996; Nairn, 2002)

Group	Name	Age (ka)	Volume (DRE)	Caldera Produced
	Quartz-biotite	550	90 km^3	Yes
	Murupara/Bonisch Pyroclastic Subgroup	340-325	30 km^3	No
	Matahina	325	160 km^3	Yes
	Onuku/Pokopoko	325-240	20 km^3	No
	Te Wairoa Pyroclastics		1 km^3	No
	Rotoiti / Earthquake Flat	45	100 km^3 / 10 km^3	Yes
Mangaone Pyroclastic Subgroup	Unit A	42.7[1]	22 km^3	No
	Unit B (Ngamotu)	39.6[1]		
	Unit C	37.7-36.6[1]		
	Unit D (Maketu)	36.1[1]		
	Unit E (Te Mahoe)	35.6[1]		
	Unit F (Hauparu)	35.2[1]		
	Unit G	33.8[1]		
	Unit H	31.8[1]		
	Unit I (Mangaone)	31.1[1]		
	Unit J (Awakeri)	31.0[1]		
	Unit K	30.8[1]		
	Unit L	30.6[1]		
Post 26 ka	TeRere	25.2[2]	13	No
	Okareka	21.8[2]	8	No
	Rerewhakaaitu	17.6[2]	5	No
	Rotorua	15.4[2]	4	No
	Waiohau	13.6[2]	11	No
	Rotoma	9.5[2]	8	No
	Mamaku	8.0[2]	17.5	No
	Whakatane	5.5[2]	13	No
	Kaharo	1314 AD[2]	5	No
	Tarawera	June 10 1886[2]	0.7	No

Table 2.2: Approximate crystal content and dominant mineralogy for eruptions selected for this study.

Eruption name	Crystal content (%)	Mineralogy
Pokopoko	15	plag, opx, hbl, Fe-Ti ox
Onuku	10	plag, opx, hbl, Fe-Ti ox
Rotoiti	20	qtz, plag, hbl, opx, Fe-Ti ox
Earthquake Flat	40	qtz, plag, hbl, opx, bio, Fe-Ti ox
Mangaone Unit B/C	5	plag, hbl, opx, cpx, Fe-Ti ox
Mangaone Unit D (Maketu)	5	plag, hbl, opx, cpx, Fe-Ti ox
Mangaone Unit F (Hauparu xstl poor)	5	plag, opx, cpx, Fe-Ti ox
Mangaone Unit F (Hauparu xstl rich)	15	plag, hbl, opx, cpx, Fe-Ti ox
Mangaone Unit I (Mangaone)	5	qtz, plag, hbl, opx, Fe-Ti ox
TeRere	15	qtz, plag, hbl, opx, Fe-Ti ox

3 Methods

3.1 Sample preparation

3.1.1 Sample selection criteria

Pumice samples from ten separate OVC eruptions were used in this study (Table 2.2). The samples were selected to represent eruptions that span a caldera forming cycle. Pumice clasts for this study were first cleaned with water and a nylon brush to remove dirt and debris. After surficial scrubbings, the pumice clasts were placed in an oven at 80 °C for 24 hours to dry. Once dried, individual pumice clasts from each eruption were selected to be crushed based on the condition of glass. Pumice clasts that exhibited discoloration that varied between the rind and interior were discarded in favor of pumice clasts that appeared to be unaffected by post emplacement alteration.

3.1.2 Crushing

Initial attempts to crush the sample were attempted via ceramic mortar and pestle. This method proved to be time consuming, and often resulted in over crushing of the sample. Alternatively, the pumice clasts were coarse crushed with a Lemaire Instruments Model 150 tabletop jaw crusher. The minimum width of the gap at the bottom of the jaw crusher was approximately 5mm, which prevented excessive crushing of the pumice samples and maximizes crystal yield from encapsulating pumice.

3.1.3 Sieving

Coarse crushed samples were placed in a nested set of brass sieves with opening sizes of 2.36, 1.00, 0.60, and 0.25 mm. The stack of sieves was then placed on a Gilson mechanical sieve shaker and set to 15 minutes of continual oscillation. Sieve products that ranged from <2.36mm and >0.25mm were bagged and winnowed to separate crystalline phases from glassy pumice (e.g.: Gualda, 2007; Skirius et al., 1990)

3.1.4 Winnowing

The winnowing process used to remove glass from crystals involved using a large beaker, a fine sieve (opening size 0.25mm) and a constant flow of tap water. The material produced from each sieve was winnowed individually to maintain the size fractions mentioned above (>2.36mm, <2.36 - >1.00mm, <1.00mm - >0.60mm, <0.60mm - >0.25mm). After adding dry sieved sample to the beaker, the beaker was held under a light to moderate flow of tap water. The beaker was then rocked back and forth above the fine sieve, allowing for low density glassy pumice to float to the top and pour out into the catchment sieve. After the bulk of the sample floated out, the water was turned off, and a gentle rocking and tipping of the beaker allowed for further removal of the material that was composed of a mix of glass and some mineral material. What remained was a reduced sieve proportion that was generally >90% mineral phases by volume. The winnowed portion was then drained and placed in a drying oven at 80 °C for 24 hours.

3.1.5 Grain selection and mounting

The winnowed crystal separates for each eruption were inspected using a binocular microscope. Crystals for each size fraction were hand-picked with binocular microscope and fine-tipped tweezers. Notable variations within crystals populations of each eruption were selected to insure representative sampling of each deposit in this study. Glomerocrysts, or phenocryst clusters, of mono- or poly- mineralic constitution, were also selected.

The mineral phases were mounted on 25mm diameter plastic plugs using double sided tape. The minerals from each eruption were mounted based on size to ensure more consistent results when the epoxy plugs were ground to a satisfactory depth and subsequently polished. A two-part epoxy was mixed and poured in the mold for each plug and allowed to cure for a minimum period of 24 hours at ~21 °C. After the cure, the plugs were removed from the molds, and ground with a Diamond Pacific flat lap. The coarse grind procedure stepped through 60-180-320-600 grits to ensure even removal of material. Once the plug was ground to a point where the majority of the mounted crystals had exposed interiors,

the plugs were hand polished using adhesive polishing pads and water lubricated diamond lap paste. A three-step polishing process used 9μ, 6μ, and 1μ. The resulting plug ideally had mirrored crystal phases with minimal scratches and rounding on the edges of the crystal.

3.2 Mineral textural characterization

3.2.1 Environmental scanning electron microscope (SEM) imaging

Imaging of plagioclase crystals was completed at the Applied Chemical and Morphological Analysis Laboratory (ACMAL) at Michigan Technological University using a Philips XL40 ESEM. Sample plugs were carbon coated to a thickness 250-300 Å prior to placement in the microscope. Plugs were placed in the sample chamber with conductive tape used to ground the coated sample surface to the stage to minimize charging.

The backscatter electron (BSE) detector equipped on the ESEM was used to produce images that elucidated the major elemental zoning patterns in the crystal cross sections exposed in each plug. An accelerating voltage of 20kV and spot size of 5 were used to optimize the imaging of the compositional zones and grain edges rather than surface topography of the grains. The contrast setting for the microscope was increased to a maximum, and brightness subsequently adjusted to a satisfactory level for each crystal. An increased dwell time was applied in addition, which resulted in final images with a greater degree of detail.

3.2.2 Grain and spot selection

Textures and zoning types in crystal populations were used to select grains for geochemical analysis. Additionally, grain size was considered so that a range of grain sizes produced from the nested sieves would be used to incorporate minerals that experienced different stages of growth in the volcanic system.

Analysis locations were mapped on crystals of interest based on the zones present in the SEM images. Every crystal was given a location for a rim and a core measurement. Interior

zones were also targeted and selected based on perceived width of the zone and context to the crystal. Zones less than 50μm across were largely ignored to avoid chemical analyses of intrazonal regions.

3.3 Geochemical analytical methods

3.3.1 Microprobe major element analysis

Major element analysis was completed at Oregon State University Electron Microprobe Laboratory in Corvallis, OR. The lab utilizes a Cameca SX-100 Electron Microprobe that is equipped with five wavelength dispersive spectrometers and high intensity dispersive crystals for enhanced analysis precision. Analyses on crystal samples were completed using 15keV accelerating voltage, 10 nA sample current, and 10 μm beam size. The microprobe was calibrated each day prior to running analyses. Appendix A provides information relating to procedure and microprobe analyses of the standard as an unknown.

3.3.2 Laser ablation and inductively coupled plasma mass spectrometry (LA-ICP-MS)

The analysis of plagioclase samples for trace element concentrations were measured using laser ablation inductively coupled plasma mass spectrometry (LA-ICP-MS) at the W.M. Keck Collaboratory for Plasma Mass Spectrometry at Oregon State University. Material was ablated from the plagioclase samples using a Photon Machines Analyte G2 193 ArF Excimer Laser. The ablation occurred using a 30 μm spot size, repetition rate of 12Hz, and shot count of 540. Ablation occurred in a He atmosphere and ablated material was carried to the Thermo Scientific iCAP-RQ ICP-MS using helium as a carrier gas. Trace element data collected was processed using LaserTram Visual Basic software using ^{43}Ca as the internal standard isotope and GSE-1G as the calibration standard (see Loewen (2013) for detailed method using LaserTram software). Results from analysis of secondary calibration standards (USGS GSE-1G, BHVO-2G and NIST SRM-612) are included in Appendix B. Accepted values for these standards were acquired from the GeoReM database (http://georem.mpch-mainz.gwdg.de/).

3.4 Modeling Methods using Polytopic Vector Analysis (PVA)

Polytopic Vector Analysis (PVA) was developed to analyze samples that are mixtures of two or more compositional end-members (EMs). This multivariate statistical tool evaluates geochemical datasets and produces an output that provides end-member compositions and proportions of each for analyses provided in the input dataset. Three parameters are needed to characterize a mixing system: 1) the number of EMs in the system 2) the composition of each EM and 3) the relative proportion of the EMs in each sample analysis. Most commonly used with whole rock compositions in igneous petrology studies (e.g.: Deering et al., 2008; Tefend et al., 2007; Vogel et al., 2008), recent studies have demonstrated the utility of this tool in studies with apatite (Lisowiec et al., 2015) and plagioclase (Słaby et al., 2017).

In order to determine the proportion and composition of each end-member, the compositional data must be plotted in the confines of a generalized geometric figure called a polytope. The polytope in PVA solutions contains a vertex for each end-member in the solution and is thus one less dimension than the number of end-members.

Prior to determining the composition and relative proportion of each EM in the samples using PVA, the number of EMs must be determined. The VSPACE module in the PVA package assists in determining an appropriate minimum number of EMs to describe the mixing relationship. The VSPACE output provides several statistical measures that are used to determine the number of EMs. The first report of importance is the cumulative variance explained by an increasing number of eigenvectors in the solution. The number of eigenvectors in the solution represents the number of vertices in the simplex that attempts to encapsulate the cloud of data. The cumulative variance values should not be used as a sole reference for selecting a potential number of end-members but provide a useful starting point.

An additional criterion useful in selecting the number of end-members is the Klovan / Miesch Coefficient of Determination (KMCD) (Klovan & Miesch, 1976). The KMCD represents the ratio between the actual data values from the input dataset and the back-

calculated values from the PVA module. Support for a given number of EMs is suggested by KMCD values that approach 1.0 for the analytes (major and trace element concentrations) in the dataset.

In such exploratory evaluations, a solution for the number of EMs in a system is difficult to subject to a rule-of-thumb cutoff criteria. For instance, not all analytes in a particular dataset may be useful for the subject in PVA. This dataset includes compositions of Ni and Cr in plagioclase. These elements do not occur in plagioclase in a significant fashion and can be considered less important than trace elements that are preferentially incorporated in crystal such as Sr and Ba. Although a solution will be created to explain the variance in less significant analytes, the number of end-members is often much greater than what is feasible to describe for a single system solution. The importance of selecting a realistic number of end-members should consider the cumulative variance explained by the eigenvectors, a KMCD value cutoff of ≥ 0.6 for analytes (see: Lisowiec et al., 2015; Słaby et al., 2017) and the geologic system that influenced the evolution of the subject. End-members represent mass contributions from potentially evolving magmas and different sources alike.

Once an appropriate number of EM is selected, the iterative process of PVA proper modifies the location of the initial polytope incrementally until all data is encapsulated within the shape, and mixing ratios are positive (or greater than user defined maximum negative value for EM proportion). In this study, the maximum allowable negative value was -0.07. Negative values in successful PVA results that occurred between 0 and -0.07 were set to 0 and proportions were then recalculated to 100%.

4 Results

4.1 Textural variation of plagioclase

Qualitative textural analysis of plagioclase crystals was conducted by categorizing grains based on patterns of BSE intensity in imaging results. BSE imagery highlights on polished crystal cross sections the differences in average composition based on atomic number. Plagioclase forms a continuous solid solution series between Ca and Na rich end-members. The difference in proportion between Ca (anorthite) and Na (albite) defines the brightness intensity of the zones in the images. Areas richer in Ca (larger atomic number) appear with a greater BSE intensity than areas with more Na (smaller atomic number) (Ginibre, Kronz, et al., 2002). Representative plagioclase images and textures are given in Figure 4.1.

4.1.1 Individual plagioclase grains

Individual plagioclase grains with solid (consistent BSE intensity) cores are found throughout the caldera cycle and are found in each eruption in this study (Table 4.1; Type 1). Crystals with solid cores and oscillatory rim sequences were the most common texture type for all eruptions. Rim sequences exhibit both normal and reverse oscillatory growth patterns. Oscillatory zones, demonstrated by changes in BSE image intensity, vary in thickness between crystals within each eruption.

Patchy core (inconsistent BSE intensity) plagioclase crystals occur in each eruption in this study (Table 4.1; Type 2). The proportion of individual grains with patchy cores is highest in the Rotoiti and Earthquake Flat pumice samples. Cores in these minerals exhibit regions of high and low BSE intensity within the core region. Rim sequences most commonly show oscillatory growth in normal and reverse patterns, but also demonstrate considerable resorption.

Individual grains also demonstrate sieve texture in the cores (Table 4.1; Type 3). This classification of plagioclase, except for four pre-caldera grains, occurs exclusively after the Rotoiti and Earthquake Flat eruptions. The sieve core plagioclase exhibit rim sequences

with normal and reverse oscillatory zoning. Rim sequences are also occasionally interrupted by grain boundaries that have eroded rim sequences.

4.1.2 Glomerocrysts

Glomerocrysts that contain plagioclase are found in each eruption in this study. The additional phases found in glomerocrysts varies based on eruption mineralogy (Table 2). The glomerocrysts are classified here using the predominate texture exhibited in the plagioclase minerals within the cluster of grains. The same three textures used for individual plagioclase grains are used to discern plagioclase in glomerocrysts.

Glomerocrysts with solid cored plagioclase (Table 4.1; Type 4) occur in each eruption in this study, with most of the clusters occurring in pumice from eruptions following the caldera forming Rotoiti eruption. Plagioclase occurs as the dominant mineral phase in most glomerocrysts. Glomerocrysts are comprised of clusters that contain one to many plagioclase grains. Solid core plagioclase crystals are most commonly euhedral in shape and share irregular boundaries with adjacent or intersecting accessory phases. The presence of Fe-Ti oxides is ubiquitous among these glomerocrysts. Biotite and amphibole occur as accessory phases in syn-caldera eruption pumice. Biotite was not found in post-caldera glomerocrysts with pyroxene as the most common accessory phase in this stage.

Plagioclase grains with patchy cores occur in a similar distribution as solid core plagioclase in glomerocrysts (Table 4.1; Type 5). Patchy core plagioclase grains were not found in glomerocrysts from Rotoiti or Mangaone Unit I pumice and were exceedingly rare in all eruptions except for Earthquake Flat. The Type 5 plagioclase mostly commonly occurs in glomerocrysts that contain numerous plagioclase grains (> 5) in the cluster and are accompanied by Fe-Ti oxides and amphibole.

Sieve texture plagioclase occur in glomerocrysts in five of the ten eruptions in this study (Table 4.1; Type 6). The trend is like those individual sieve grains, where most of the grains occur in post-caldera eruption pumice. Mangaone Unit B/C and Unit I pumice did not yield

any glomerocrysts with sieve textured plagioclase. The occurrence of this plagioclase texture occurs primarily in the Hauparu deposit.

4.2 Major element chemistry

Average element compositions for the OVC plagioclase in this study are listed in Table 4.2. Although ranges in major element composition overlap throughout the eruptions in this study, systematic changes in average compositions between eruptions are noted. Complete major element data from electron microprobe analysis provided in Appendix C.

Plagioclase from pre-caldera eruptions (Pokopoko and Onuku) contain the lowest average anorthite content of all eruption in this study ($An_{32.1}$ and $An_{35.4}$ respectively). They ranged in compositions from $An_{19.0\text{-}58.5}$ and $An_{22.8\text{-}61.0}$ respectively. Plagioclase from Rotoiti and Earthquake Flat deposits have an average An content that is slightly higher than the previous eruptions (37.9 and 36.9 respectively). The range of anorthite content for Rotoiti is slightly restricted compared to previous eruptions and Earthquake Flay ($An_{24.2\text{-}57.3}$). Earthquake Flat produced a range from $An_{22.1\text{-}63.3}$. Following caldera formation from the Rotoiti event, plagioclase from early Mangaone Subgroup eruptions exhibit a marked increase in average An composition. Average anorthite content in Mangaone Unit B/C ($An_{39.9\text{-}67.2}$) through Hauparu (crystal poor: $An_{32.0\text{-}65.8}$, crystal rich: $An_{22.9\text{-}68.8}$) range from 48.2 to 51.2, with the highest average occurring in Mangaone Unit B/C plagioclase. Mangaone Unit I plagioclase break from the high An trend, with an average of $An_{39.5}$ and a range of $An_{23.4\text{-}54.2}$.

Trends in FeO and MgO (Figure 4.1a, b) exhibit similarities to those seen in anorthite. System low averages in these elements are seen in pre-caldera plagioclase from Pokopoko and Onuku. Syn-caldera plagioclase demonstrate an adherence to pre-caldera trends, with average concentrations leveling off during the syn-caldera events. Following caldera formation, the onset of volcanism in the early Mangaone Subgroup produced plagioclase with high averages FeO and MgO content. Although Maketu through Hauparu have high averages in these elements, they also produced analyses with low concentrations like those

found in sieve plagioclase glomerocrysts. The trend towards pre / syn-caldera plagioclase is observed in Mangaone Unit I and TeRere in respect to FeO and MgO content.

K_2O content in these plagioclase changes in a fashion unlike other major element analytes (Figure 4.1c). A systematic decrease in average K_2O is seen from pre-caldera plagioclase to Rotoiti. The range in K_2O content in Rotoiti plagioclase is restricted compared to pre/syn-caldera plagioclase (0.12 – 0.49 wt%), while Earthquake Flat plagioclase exhibit a large range of K_2O content (0.11 to 0.94 wt%) and the highest average K_2O composition out of all eruptions in this study (0.47 wt%). A drop in average K_2O composition occurs following caldera formation (Mangaone Unit B/C average K_2O wt% = 0.16) and is followed by a gradual increase through the remainder of the Mangaone Subgroup (Mangaone Unit I average K_2O wt% = 0.27). Maketu, Hauparu crystal rich, and Unit I all contain several plagioclase analyses enriched in K_2O (greater than 0.5 wt%) that overlap with Earthquake Flat and pre-caldera plagioclase.

4.3 Trace element chemistry

Trace element concentrations exhibit differing evolutionary patterns through the caldera forming cycle (Table 4.2, Appendix D). An enrichment of Ba in plagioclase occurs in eruptions through pre and syn-caldera eruptions. Beginning with Mangaone Unit B/C, plagioclase predominately demonstrate a depletion in Ba concentration (Figure 4.2d). It is important to note that there is some compositional overlap in respect to Ba between pre and post-caldera eruptions. There is also a clear divergence in respect to Ba vs. An content. Pre and to an extent syn-caldera plagioclase occurred along a low An / high Ba to high An / low Ba trend. Early post-caldera plagioclase chemistry shows a flat slope trend from high An / low Ba to low An / low Ba. Late post-caldera plagioclase chemistry adheres to a trend more similar to pre-caldera plagioclase. The opposite trend is exhibited in respect to Sr concentrations. Pre and syn-caldera forming eruptions show more heterogeneity and are more depleted on average than post-caldera eruptions in the Mangaone Subgroup and TeRere (Figure 4.2e)

Yttrium concentrations gradually increase from pre-caldera eruptions through the early Mangaone Subgroup until Maketu where concentrations stabilize between 0.25 and 0.5 ppm, with Mangaone Unit I and TeRere settling slightly on average towards Mangaone Unit B/C Y compositions. Apart from two analyses from Rotoiti, a population of zones from post-caldera plagioclase (n=21) have high Y concentration (Y > 1ppm).

The change in Eu through time in OVC plagioclase demonstrates a trend that closely mirrors the changes in Ba (Figure 4.1f). Mean Eu concentrations decrease from Pokopoko through Rotoiti (Pokopoko: 3.11 ppm, Onuku: 1.98 ppm, Rotoiti:1.57ppm). Earthquake Flat interrupts the depletion trend temporarily with a large range of Eu with a mean concentration of 2.03 ppm. Mangaone Subgroup Eu characteristic changes abruptly at Mangaone Unit I. Early Mangaone plagioclase (Unit B/C – Hauparu) occur in a narrow range of concentrations, with averages between 1.25 – 1.57 ppm. Mangaone Unit I and TeRere show enriched Eu behavior with both averages occurring above 2 ppm.

Light Rare Earth Elements (LREE; La, Ce, Pr) exhibit trends of systematic increase from Pokopoko to Earthquake Flat. The range of compositions through this sequence of eruptions generally increase as the eruptions occurred, with Earthquake Flat exhibiting the largest heterogeneity in LREE. With a range of La between 1.97 – 19.6 ppm, Earthquake Flat plagioclase nearly contains the entire compositional range of OVC plagioclase in respect to La. Compositional range is strictly reduced in the Mangaone Subgroup with the slight exception of Hauparu crystal rich, which resembles pre-caldera heterogeneity, but with a lower average LREE composition in line with Mangaone Subgroup plagioclase. LREE trends show an uptick in enrichment in Mangaone Unit I and TeRere plagioclase, which is also seen with MREE such as Eu.

4.4 PVA results for OVC

The PVA module generates several outputs that aids in determining an appropriate number of end-members to explain the sample population (Appendix E). Cumulative variance values of 95% and 98% occurred at four end-members and eight end-members respectively for this dataset. KMCD values for each analyte at a given number of end-members can be

viewed similarly to the r^2 values used in regression analysis. An arbitrary lower limit of 0.6 is used here but has been assigned lower values such as 0.4 (Szymanski et al., 2013). Of the 23 analytes used in the PVA dataset, 16 have at least a minimum value of 0.6 at four end-members while 19 surpass the lower limit at eight end-members. The number of analytes with a value greater than or equal to 0.8 is reduced to ten for a four end-member solution, and seventeen for an eight end-member solution.

A four end-member solution was selected to represent the minimum number of end-members required to explain the chemical variation in this plagioclase population. A four-end-member solution produced a high cumulative variance value (>95) and a minimum acceptable KMCD value (0.6) for the majority of high importance elements. Although solutions with additional end-members do produce higher KMCD values for analytes, the resulting compositions of the end-members in these solutions become unrealistic and redundant. The compositions of the four end-members are provided in Table 4.5. The four end-member solution produced one high, one low, and two intermediate compositions based on calculated anorthite content. EM1 (An77) is enriched in FeO and MgO and contains a depleted trace element profile, but shows moderate concentrations of Sc, Cr, Ni, Sr, and Y. EM2 (An0) has the most depleted trace element profile out of the four end-members, with only a slight Ba concentration. EM3 and EM4 are characterized by moderate anorthite contents (An59 and An49 respectively). EM3 is moderately enriched in FeO and MgO and is characterized by moderate enrichments in the trace elements. This EM contains a relative e enrichment of Y (0.981 ppm). EM4 is depleted in FeO and MgO but contains an enriched trace element profile. Besides Ni, Y, and Gd, EM4 contains the highest concentration of all trace elements in the PVA results. Contributions from each end-member for the samples in the dataset are provided in Appendix E.

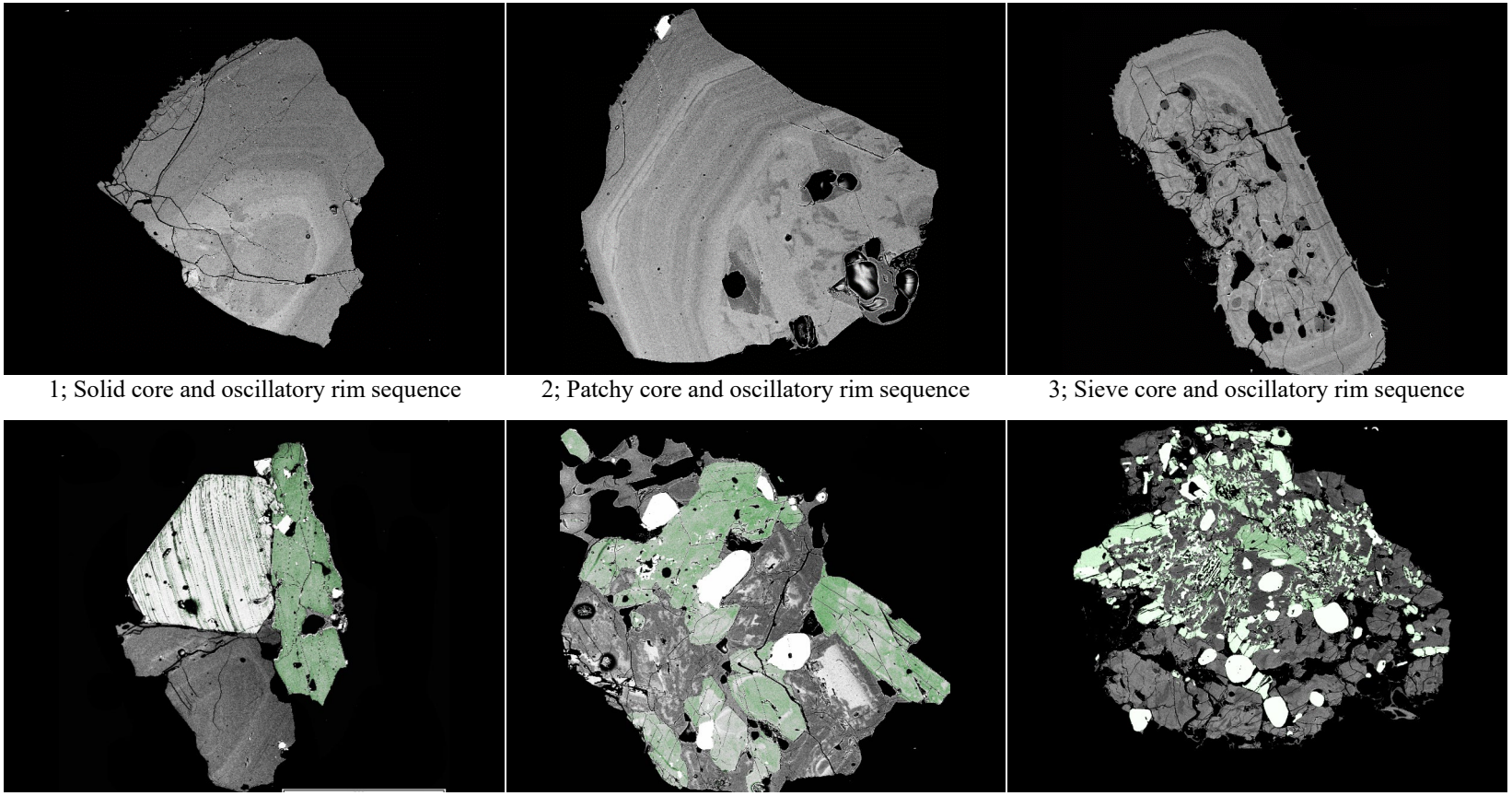

1; Solid core and oscillatory rim sequence | 2; Patchy core and oscillatory rim sequence | 3; Sieve core and oscillatory rim sequence

4; Solid core plagioclase in glomerocryst | 5; Patchy core plagioclase in glomerocryst | 6; Sieve plagioclase in glomerocryst

Figure 4.1: Textural classification of OVC plagioclase. Glomerocrysts textures are based solely on plagioclase characteristics. False color images for glomerocryst grains are provided to differentiate between plagioclase (shades of grey) and other accessory minerals (shades of green or pure white).

Eruption	Pokopoko	Onuku	Rotoiti	Earthquake Flat	Mangaone Unit B/C	Maketu	Hauparu xstl poor	Hauparu xstl rich	Mangaone Unit I	TeRere
n =	88	77	149	127	87	140	123	137	77	79
SiO_2	60.311	59.581	58.954	59.226	55.707	56.489	56.371	56.454	58.537	57.345
Al_2O_3	24.849	25.432	25.837	25.618	27.810	27.359	27.336	27.383	26.051	26.714
TiO_2	0.011	0.008	0.009	0.011	0.019	0.023	0.021	0.020	0.012	0.018
FeO	0.231	0.189	0.215	0.236	0.377	0.401	0.388	0.391	0.268	0.341
MgO	0.007	0.006	0.009	0.010	0.032	0.033	0.033	0.031	0.012	0.025
CaO	6.454	7.101	7.613	7.420	10.247	9.714	9.691	9.654	7.920	8.898
K_2O	0.454	0.420	0.284	0.479	0.163	0.211	0.207	0.227	0.275	0.226
Na_2O	7.220	6.883	6.686	6.664	5.284	5.561	5.549	5.570	6.510	5.989
Sc	6.717	6.171	6.742	7.798	5.225	6.362	6.355	6.177	6.302	5.123
Cr	0.957	1.058	1.057	0.993	1.054	1.083	1.115	1.003	0.870	1.030
Ni	0.034	0.074	0.057	0.066	0.073	0.091	0.113	0.096	0.067	0.067
Rb	0.744	0.615	0.440	0.974	0.359	0.262	0.345	0.438	0.404	0.682
Sr	638.700	630.888	668.548	632.303	790.962	752.417	751.920	718.602	744.791	797.336
Y	0.270	0.265	0.299	0.304	0.398	0.435	0.438	0.443	0.393	0.470
Ba	530.105	450.408	377.824	570.374	178.553	180.167	209.614	201.989	276.788	267.097
La	6.580	7.567	7.566	9.301	4.372	4.123	4.700	4.392	6.004	5.777
Ce	8.635	9.621	10.223	11.999	6.585	6.369	7.094	6.665	8.865	8.419
Pr	0.756	0.804	0.863	0.965	0.641	0.629	0.689	0.643	0.816	0.793
Pm	0.551	0.545	0.586	0.626	0.504	0.512	0.542	0.498	0.620	0.613
Nd	2.402	2.411	2.594	2.812	2.181	2.225	2.414	2.240	2.688	2.666
Sm	0.211	0.221	0.218	0.218	0.240	0.264	0.254	0.246	0.272	0.276
Eu	3.111	1.985	1.574	2.032	1.252	1.443	1.558	1.338	2.080	2.061
Gd	0.096	0.088	0.111	0.110	0.138	0.163	0.163	0.155	0.166	0.200

Table 4.1: Average plagioclase composition (n = number of analyses) for each eruption in OVC caldera forming cycle. Major elements are provided in wt%. Trace elements are provided in parts per million (ppm) concentration. See Appendix C and D for complete major and trace element tabulations.

Table 4.2: Composition of each member of a 4 EM solution. Major element concentrations are in wt%, trace element concentrations in ppm.

Analyte	EM 1	EM 2	EM 3	EM 4
SiO_2	49.00	70.60	53.70	55.30
Al_2O_3	32.00	16.90	29.20	28.50
TiO_2	0.05	0.00	0.03	0.00
FeO	0.70	0.00	0.48	0.00
MgO	0.07	0.00	0.04	0.00
CaO	15.50	0.00	11.90	10.10
K_2O	0.00	1.22	0.00	0.00
Na_2O	2.55	11.30	4.57	5.74
Anorthite	0.77	0	0.59	0.49
Albite	0.23	0.93	0.41	0.51
Orthoclase	0	0.07	0	0
Sc	4.57	0	5.14	20.5
Cr	1.24	0.0735	0.908	2.19
Ni	0.161	0.0415	0.158	0
Rb	0	0.152	0.879	2.4
Sr	904	0	983	1360
Y	0.385	0	0.981	0.56
Ba	0	234	184	1710
La	0	0.507	6.79	30.6
Ce	0	0	11.5	38.6
Pr	0	0	1.18	3.05
Pm	0.0274	0	0.991	1.97
Nd	0.272	0	4.22	8.71
Sm	0.13	0	0.572	0.613
Eu	0	0.906	2.36	6.09
Gd	0	0.0159	0.925	0

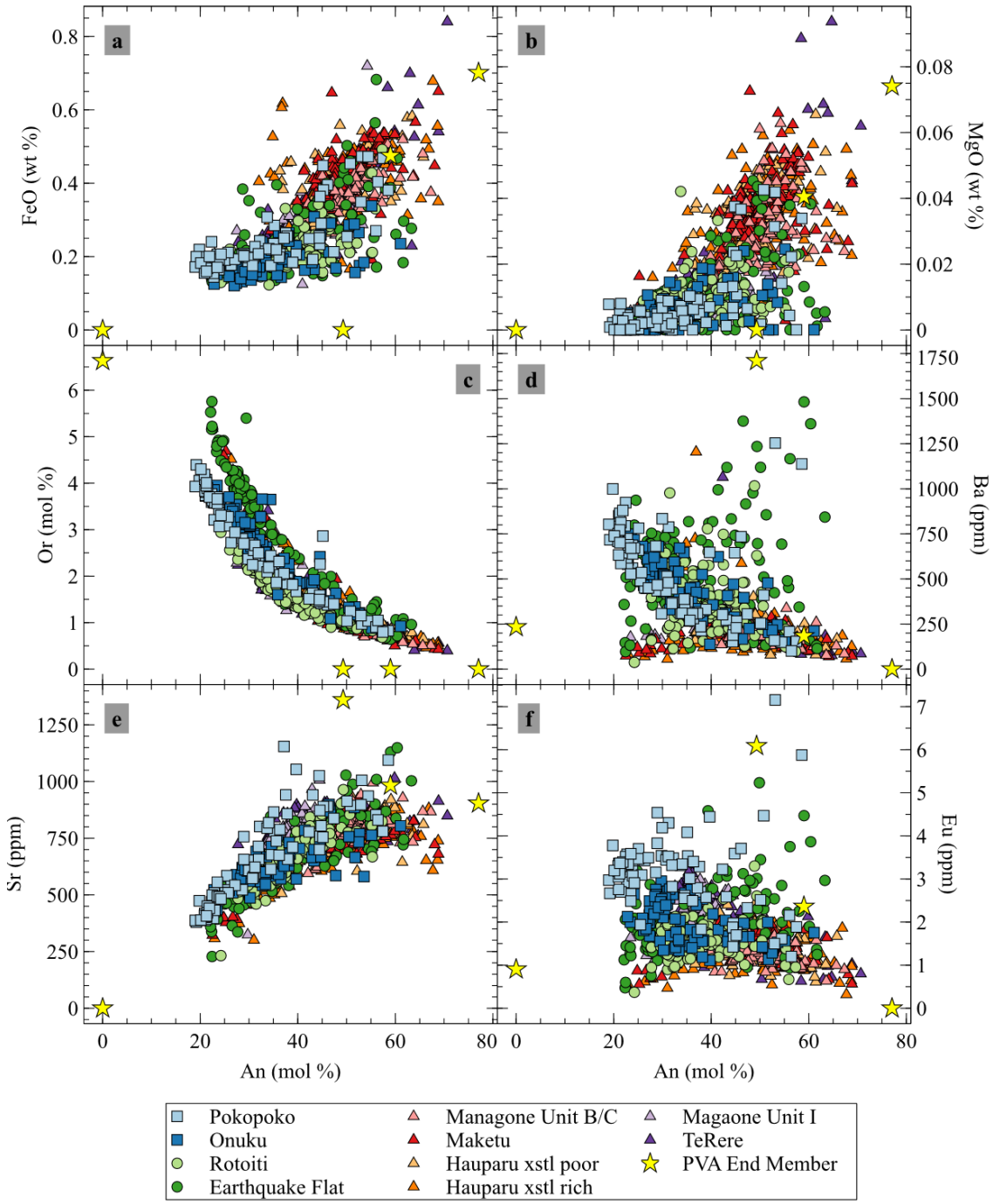

Figure 4.2: a-f: Bivariate plot matrix of major and trace element chemistry results for OVC plagioclase. Anorthite content is the common x-axis for all six plots.

5 Discussion

Some of the largest calderas on Earth have formed in arc volcanic settings (e.g., Best et al., 2016; Hughes & Mahood, 2008; Melnick et al., 2006). Calderas are formed by the evacuation of large volumes of silicic magma that was assembled and stored in an upper crustal reservoir. These large eruptions clearly pose a significant threat to modern society, therefore, determining the conditions and signs that precede these potentially devastating events has been the subject of many studies. In particular, there has been a recent focus on determining the periods when the magmatic system is in an 'eruptible' state; considered to be magma with less than 50% crystals. Magma in systems that are beyond 50% crystalized becomes rheologically hindered and unlikely to erupt (Marsh, 1981). For those volcanic systems that are in the midst of a caldera forming cycle, we can evaluate the physical state of the magmatic system by analyzing plagioclase crystals produced from eruptions during the most recent caldera cycle to postulate where the system is now.

In particular, plagioclase crystals can offer a more detailed representation of the magma evolution as it is a liquidus phase that preserves the compositional characteristics of the reservoir. Although age dating intracrystalline growth zones in plagioclase is not possible in the way that it is for other phases such as zircon, plagioclase can still demonstrate temporal changes to a magmatic system through a caldera cycle. Here we assess the changes in the thermo-mechanical state through the most recent OVC caldera cycle by utilizing chemical, textural and statistical information derived from the plagioclase at OVC.

5.1 The thermo-mechanical evolution at Okataina

The primary factor that influences the 'eruptibility' of a magmatic system is its physical state. Similar to other silicic volcanic centers, the eruptible magmatic system in the upper crust at Okataina has been described as a crystal mush that is comprised of a crystal framework supported by interstitial melt (Andersen et al., 2019; Bachmann et al., 2011; Deering, Cole, et al., 2011; Klemetti et al., 2011). Although these mush systems are often cited to describe the physical status of a wide array of volcanic systems, the understanding of the evolution of these mush systems through time is still a topic of debate. The

mechanical state that these upper crustal magma bodies exist in has been subject of debate between a “cold” and “warm” storage where the eruptibility is controlled by the crystallinity and viscosity of the magma (e.g.: Barboni et al., 2016; Cooper & Kent, 2014; Rubin et al., 2017).

The interactions between reservoirs can be characterized generally by a spectrum of hybridization that is controlled by the input of primary, less evolved magma and the degree of crystallization of the magma in the host reservoir (Figure 5.1). Here, low degree of host crystallization, akin to a warm storage environment, lends to more complete mixing with intruded mafic material (Column 1) while near complete crystallization of the reservoir, akin to a cold storage environment, encourages dike propagation of less evolved intruded material through the host reservoir (Column 4). Magma mingling (Column 2) and Composite dikes (Column 3) occur when intruded magma can mingle and mix with the host reservoir to varying degrees (Barbarin & Didier, 1992).

5.1.1 Textures

Variations in growth zone textures occur because of changes in P-T-X conditions of the melt in which a crystal resides. Crystals that have a solid core and oscillatory zones are noted in each eruption within this series (Table 4.1:1). Small scale (width and ΔAn) zoning oscillations have been shown to reflect local changes in the boundary layer kinetics during equilibrium interactions between melt and crystal, while large scale (zone width and ΔAn) oscillations suggest more significant changes to the P-T-X conditions of the magmatic system (e.g.: Pearce & Kolisnik, 1990; Ruprecht & Wörner, 2007; Viccaro et al., 2009). These larger scale fluctuations often accompany unconformities in the zoning stratigraphy in response to intrusions of hotter, less evolved melt. The variations in zoning amplitude and frequency are often not mutually exclusive in each population of plagioclase however, as each eruption often produces plagioclase with a complex variety of growth textures.

Patchy zoning is considered here to indicate a change in environmental parameters surrounding an existing crystal such that it was no longer in equilibrium with the surrounding melt. As a result of the disequilibrium, the plagioclase reacted with the host

melt, partially dissolved, and subsequently grew from a melt with different characteristics than the melt that the core of the crystal originally grew in (Nakamura & Shimakita, 1998)(Table 4.1:2). These cores are characterized by a bimodal An content (rich and poor) (e.g. Sas, 2020; Streck, 2008). Previous research has suggested either partial dissolution of a high Ab crystal and subsequent infilling of a high An content or dissolution of a high An and subsequent infilling of high Ab content. The most compelling explanation for the majority of the patchy OVC plagioclase is that a high An plagioclase partially dissolved and was infilled by low An plagioclase. This mechanism is consistent with less evolved plagioclase being transported to a shallower, more evolved part of the magmatic system, partially dissolving before growing in the more evolved melt.

Sieve textured plagioclase have been shown to form in a variety of magmatic environments that cause partial dissolution of the crystal. One method for plagioclase dissolution has been postulated to occur when a sodic plagioclase reacts with a less evolved calcic melt (Tsuchiyama, 1985). Another method cites that decompression during rapid transport of plagioclase in water undersaturated mafic magma can cause destabilization and subsequent dissolution of plagioclase (Nelson & Montana, 1992). Though the determination of the exact method behind the formation of the sieve textures in this system is beyond the scope of this paper, the common theme of ascent and introduction of mafic magma to an evolved upper crustal magma is integral to the interpretation of this texture. It is worth noting that this sieve texture does occur in more than one pattern. The two main patterns include 1.) a sieve core that is encapsulated by an oscillatory rim growth sequence (Table 4.1:3) and 2.) a sieve plagioclase grain which contains accessory minerals in the voids that define the sieve texture (Table 4.1:6).

Glomerocrysts, or clusters of multiple crystals, are ubiquitous in many igneous provinces around the world (Table 4.1:4 & 5). In a system that is described as a magmatic mush, glomerocrysts likely represent remobilized crystal cumulates (Molloy et al., 2008; Wolff et al., 2015). The occurrence of glomerocrysts, both monomineralic and polymineralic, occurred throughout the eruptive cycle. The presence of these grains in eruption deposits

provide insight about mobilized portions of the mush in the eruptive portion of the magma reservoir.

5.1.2 Geochemistry

Minerals such as plagioclase are dutiful recorders of more nuanced changes of their surroundings when compared to bulk rock ejecta and provide a more refined record of magmatic conditions. Due to the incremental nature of magmatic crystal growth, conditions of magmatic systems are periodically recorded by growing crystals when conditions permit crystal growth. The chemistry of the crystal is dependent on several factors include the pressure and temperature of the magmatic system and the composition and H_2O content of the melt (Housh & Luhr, 1991). The successive growth of the mineral, which likely occurs during discontinuous episodes that punctuate long periods of sub-solidus system conditions, provide more information about the development and maintenance of the magmatic system between eruptions (Rubin et al., 2017).

Although the major element chemistry in plagioclase crystals commonly mirrors the trends of major element chemistry of the bulk rock, trace element concentrations in plagioclase are not unequivocally controlled by major element composition and thus can illuminate additional detail about the dynamics between melt and growing crystals. Partition coefficients (Kd value) describe the preference for a given element to be incorporated in a mineral. Compatible elements, which have a Kd value greater than 1, are preferentially accepted by the mineral, while incompatible elements (Kd value less than 1) meet opposition to incorporation into the solid and reside in the melt. Table 5.1 lists common fractionating phases from the OVC and their reported Kd values from studies of rhyolitic rocks. Previous trace element modeling in the OVC using whole rock data demonstrated that a varying ratio of hornblende – pyroxene fractionation is sufficient to explain the variation of chemical compositions seen in the OVC rhyolite (Deering, Bachmann, et al., 2011). This solution describes a system that varies between a hot dry reducing magma driven by low fluid flux that is earmarked by fractionation of pyroxene and high Y content and a cool wet oxidizing magma that lacks the high Y content and is the result of hornblende fractionation. This platform is used here with minor adjustments based on the

influence biotite may have had in addition to pyroxene and hornblende in the system's evolution.

5.1.3 PVA

PVA is a utility utilized by petrologists to help compartmentalize the chemical variability that occurs in magmatic systems. In several studies, this multivariate approach has proven valuable in defining geochemical end-members and highlighting more subtle variations in whole rock data sets (e.g.:Deering et al., 2008; Szymanski et al., 2013; Tefend et al., 2007; Vogel et al., 2008). However, its utility in delineating crystal chemistry has seldom been assessed. It is worth noting here that with any PVA result, the end-member compositions that are generated do not necessarily represent actual chemical compositions that existed in the system but rather represent vertices required to encapsulate the chemical variation of the input dataset.

PVA results for this plagioclase dataset indicate that a minimum of four unique chemical end-members are required to describe the chemical heterogeneity in the population of plagioclase compositions. The four end-members are broadly characterized by their An content. EM1 has the highest An content in the solution (An77) and is classified as a high temperature, less evolved mafic type chemical reservoir. EM2 is generalized as a more evolved (An0) low temperature silicic end-member. EM3 and EM4 are similar in An content (An59 and An49 respectively) and can both be classified as intermediate end-members. The distinction between the two end-members can be explained by a change in the predominate fractionating phases in the system. Partition coefficients for major minerals considered to drive changes in melt compositions at OVC are plagioclase, opx, cpx, hornblende, and biotite (Table 5.1). Due to relative concentrations in Sr, Y, and REE and previous work on EM constraints made by Deering et al. (2008, 2011), the supposed reservoir represented by EM3 likely indicates a chemical reservoir that was influenced by hornblende ± biotite fractionation and EM4 from fractionation of clinopyroxene ± orthopyroxene.

In addition to end-member compositions and their contributions to each sample, the degree of mixing between end-members can be assessed by calculating the correlation coefficient, similar to a r^2 value, for each pair of end-members in the solution (e.g.: Szymanski et al., 2013; Tefend et al., 2007; Vogel et al., 2008). A good correlation between end-members, arbitrarily defined as any value greater than 0.6 in this study, implies mixing between the end-members (Table 5.2, Figure 5.3). The degree of mixing between these chemical end-members, recorded during plagioclase growth through time, provides evidence that the storage conditions and interconnectedness with the magmatic system at OVC fluctuated through the caldera cycle (Figure 5.3).

5.2 Pre-caldera magmatic system characteristics

Preserved eruption deposits between Matahina and prior to the most recent caldera forming eruption at OVC are limited. Although these deposits may have been largely lost during the Rotoiti event, the dearth of distal OVC sourced tephra units between the caldera collapses induced by the Matahina and Rotoiti eruptions suggests a quiescent period that occurred between the previous two super eruptions (Cole et al., 2010).

The Pokopoko and Onuku eruptions tapped the magmatic system at OVC prior to Rotoiti and produced the highest silica rhyolites in this sequence (75.8 wt% and 76.31 wt% respectively) (Deering et al., 2008, 2010). Plagioclase from these eruptions record evidence of growth in this high silica system with the lowest average An content in the study (Pokopoko: An32; Onuku: An35) (Table 4.2). The residence and growth of these plagioclase crystals occurred primarily in the high-silica reservoir; however, evidence from both eruptions suggests that the high-silica reservoir was not the only contributor to the system during plagioclase growth.

Ba concentrations in respect to An content demonstrate a clear low An high Ba – high An low Ba trend (Figure 4.2 d). This trend is to be expected as Ba is generally incompatible in major co-crystallizing phases such as pyroxene, hornblende, and quartz (Table 5.1). As anorthite content decreases in plagioclase, the partition coefficient increases for Ba and Ba concentration in the melt is generally elevated unless biotite and/or alkali feldspar

fractionate, which leads to increases in Ba content in more evolved plagioclase. Influx and potential mixing of mafic material (high An – low Ba) would drive the melt composition back towards high An – low Ba plagioclase, while crystallization during this time would drive the melt towards low An – high Ba compositions. Mixing between these two reservoirs is further supported by the high correlation coefficient for EM1 (mafic) and EM2 (silicic) from the PVA results.

Both eruptions from this pre-caldera group contain populations of crystals that exhibit both sieve and patchy cores with normal oscillatory rim growth sequences (Type 2 and 3; Table 4.1). These textures preserve evidence of changes to the growth environment surrounding individual grains. This could either be explained by transportation of grains from one T-P-X region to another or change of environment surrounding a crystal within a single region within the mush. Ascent of mafic melt and entrained plagioclase to an upper-level silicic chamber would require a relatively solid intermediate mush zone (Figure 5.1: Column 3 or 4). The poor mixing relationship between EM1 and EM3/EM4 supports the interaction between ascending mafic magma and intermediate reservoirs was limited, which permitted mafic magma interaction with a silicic reservoir. The intruding mafic magma would have introduced juvenile plagioclase grains that reacted with new T-P-X conditions, thus creating plagioclase with a variety of core textures. New plagioclase grown in the silicic reservoir would maintain solid cores and record incremental changes in melt composition in similar oscillatory rim sequences seen transported sieve and patchy core plagioclase.

5.3 Syn-caldera magmatic system characteristics

The eruptions associated with the most recent OVC caldera collapse are preserved in the Rotoiti and Earthquake Flat deposits. Although the erupted volume of Rotoiti (~120 km^3) induced the caldera collapse and is an order of magnitude larger than Earthquake Flat (~10 km^3), both eruptions appear to have been spurred along by an increase of basaltic magmatism and intrusion into the upper crustal magmatic system (Smith et al., 2010). Both eruptions in this group are defined by crystal-rich high silica rhyolites. Rotoiti produced rhyolite from two distinct magma types, defined by the ferromagnesian crystal population

(cummingtonite in early stages, biotite and high-K plagioclase in the later stages, which is clearly mixed in intermediate stages of the eruption event (Molloy et al., 2008)). Late stage Rotoiti whole rock ejecta is like that produced during the EQF event in composition and predominant mineralogy (Schmitz & Smith, 2004; Smith et al., 2010).

The chemistry of the plagioclase broadly agrees with the changes reported in the trend of bulk rock compositions (Schmitz & Smith, 2004). The plagioclase reported here are slightly less evolved than the pre-caldera plagioclase (Rotoiti and EQF average: An37), suggesting that like the whole rock conclusions, the magmatic system was progressively influenced by the an influx of mafic magma (Smith et al., 2010; Molloy et al., 2008; Schmitz and Smith, 2004). The trace element compositions in the syn-caldera plagioclase indicates a much more complex problem however. The syn-caldera plagioclase exhibit a larger range of rare earth element (REE) compositions at given An content than the pre-caldera plagioclase. This quality is predominant in LREE content and to a lesser degree MREE (Fig. 4.2d, f). Although it appears that the majority of the REE behave in a similar fashion as pre-caldera plagioclase (i.e., high An low Ba to low An high Ba), there are two groups of analyses that span in a direction nearly perpendicular to the compositional trend defined by pre-caldera (high An & high REE / low An & low REE). This addition of plagioclase compositions in a trajectory unlike the pre-caldera plagioclase indicates an additional active reservoir recorded in plagioclase growth zones during the build up to the Rotoiti event.

The average contribution for each end-member did not fluctuate significantly during the pre and syn-caldera but the degree of mixing between EMs decreased markedly for the Rotoiti and EQF system as recorded by plagioclase (Figure 5.2 and Figure 5.3) Mixing relationships between end-members demonstrate that the once mainline relationship between mafic and silicic reservoirs prior to Rotoiti was greatly impeded in the record of syn-caldera plagioclase. The mixing between end-members was reduced to a cycle low during the development of the syn-caldera plagioclase. A high mixing coefficent between EM1 (mafic) and EM3 (hbl ± cmgt ± bio intermediate) only occurred once in this cycle during Rotoiti. This shows that in the Rotoiti magmatic system, mixing between the mafic

end-member occurred with a less evolved and likely deeper reservoir than in the pre-caldera system. This deepening of mixing alludes to an upper magmatic system that was potentially in a more liquid state; primed for a larger scale eruption. Due to density contrasts between the mafic magma and overlying wet mush, ascent and subsequent mixing was limited if not completely obscured from occurring at a shallower depth (Figure 5.1: Column 1 and 2). The conspicuous deficiency of sieve textured plagioclase from Rotoiti and EQF provide further support that the system was in a state that prohibited rapid ascent of intruded melt and associated crystal cargo during the assembly of the eruptible magma. Instead, crystals grew in a laterally and vertically extensive wet mush that was largely buffered from drastic changes in T-P-X during assembly. The dearth of sieve textured plagioclase also suggests that the plagioclase entrained in the eruptions were evacuated quickly and were not able destabilize during eruption. (J. Blundy & Cashman, 2001; Nelson & Montana, 1992).

This evidence is consistent with a laterally and vertically extensive region of eruptible magma that existed during the assembly of the caldera forming volcanic system (Klemetti et al., 2011). During this time, a large chemically heterogenous province was warmed enough to allow crystal growth in a system that did not experience significant periods of depressurization or vertically extensive intrusions of mafic magma. This encouraged the growth of chemically heterogenous crystals in a thermobarometrically stable environment which produced a limited variety of zoning patterns.

5.4 Post-caldera magmatic system characteristics

Activity following the caldera formation began a short time after the Rotoiti and EQF eruptions. The Mangaone Subgroup began ~44 ka and lasted until ~30ka (Danišík et al., 2020; Jurado-chichay & Walker, 2000). This sequence began as rhyodacite eruptions immediately following Rotoiti (Unit A – Unit F) and transitioned to high-silica rhyolite eruptions towards the end of the subgroup (Unit H – L) (Jurado-chichay & Walker, 2000; V. C. Smith et al., 2002). The higher frequency of eruptions and less-evolved chemical characteristic has been attributed to a restructuring and potentially a remobilization of parts

of the volcanic reservoir in response to the large evacuation of material during the caldera formation (e.g. Bachmann et al., 2011; Klemetti et al., 2011; Rubin et al., 2016).

In general, the sequential transition of these post-caldera plagioclase from high anorthite to low agrees with the results from prior analysis of the bulk rock chemistry (Smith et al., 2002). Evidence from zircons was used to suggest that the process for melt generation at OVC did not change significantly between pre- and post-caldera volcanism, but the interconnectedness of the magmatic system became reduced following caldera formation (Rubin et al., 2016). Although that study did not include any Mangaone Subgroup samples (Rotoiti, TeRere, Whakatane, Kaharoa), the plagioclase here confirm that the magmatic system experienced a fundamental shift following the caldera formation.

Plagioclase entrained in the old Mangaone eruptions (Unit B/C, Maketu and Hauparu) exhibit a large range of zoning textures. This includes the recurrence of sieve textured grains (Type 3 and 6; Table 4.1), grains with significant resorption events in the layer stratigraphy, and large amplitude/ low frequency oscillatory growth zones. Large oscillations in An content have been shown previously in Hauparu plagioclase and attributed to an open magmatic system that was subject to repetitive recharge of mafic magma (Shane, 2015). The mafic recharge cited as the main driver for the eruptions in this era of magmatism was able to intrude into the upper crustal magmatic system without significant hindrance from an intermediate mush that was present during the syn-caldera system. Any remainder of an intermediate mush may have become mostly solid due to rapid solidification initiated by caldera collapse and the associated pressure decrease (i.e. pressure quench; Candela (1991)), thus eliminating the density trap imposed on ascending magma (Figure 5.1; Columns 3 & 4). This is supported by the mixing relationship between EM1 and EM2 that was reestablished during the Maketu eruption and continued through the remainder of the Mangaone Subgroup and into the post-22 ka eruptions (TeRere) (Figure 5.3).

The younger Mangaone Unit I and TeRere eruptions both contain plagioclase gains that were produced in a system that was more evolved than the old Mangaone eruptions. The

younger eruptions produced plagioclase that shared geochemical similarities and a narrowed textural range like the pre and syn-caldera plagioclase. Several differences in plagioclase chemistry; however, suggest that fundamental alterations to the magmatic system occurred following the caldera collapse. Post-caldera plagioclase crystals include a significant population of high Y analyses that were essentially absent prior to the caldera formation. This high Y group has previously been suggested to indicate hotter, drier magma in the OVC and occurred primarily between 40 – 20 ka (Deering et al., 2011; Klemetti et al., 2011). In this study, the high Y end-member (EM3) so happens to be the end-member that is depleted in Ba and LREE. The elevated yet subordinate contribution of this intermediate end-member suggests that the reservoir was not a primary magma but was one that was slowly reactivated following the caldera formation.

The gradual increase in more evolved plagioclase does not follow the trend that controlled the pre-caldera plagioclase evolution. Pre-caldera and a subset of syn-caldera plagioclase evolved towards a high Ba / low An content (Figure 4.1d). Analyses from plagioclase in eruptions after the caldera formation demonstrate an inflection point along the trend of plagioclase evolution at ~An_{40}. Plagioclase zones with less than An_{40} in the post-caldera OVC were limited to low Ba concentrations rather than previous high Ba with low An. The trend of Ba concentrations in the TeRere plagioclase lacks the marque inflection point of the Mangaone Subgroup and appears on the same trend line as pre-caldera plagioclase crystals, albeit more An rich on average than pre-caldera plagioclase. The occurrence of the evolved plagioclase with low Ba demonstrates a unique evolutionary path for OVC plagioclase that occurred in response to the Rotoiti and EQF eruptions. One possible explanation for the evolved low Ba plagioclase is growth from a residual melt that was chemically controlled by the phases in which Ba was compatible. Barium is a compatible element in both biotite and potassium feldspar (Table 5.1), which in turn lowers the concentration of Ba in the melt (Figure 8b; Blundy & Shimizu, 1991). Although there is conspicuous absence of potassium feldspar in OVC pumice, this mineral has been recognized in biotite granite plutonic lithics transported in the Rotoiti eruptions (Brown et al., 1998). The presence of biotite and potassium feldspar in the deep roots of the Rotoiti system would have had a significant control on the Ba content of the resulting melt.

Extraction of a small amount of melt from a biotite / alkali feldspar cumulate during the recovery of the magmatic system following the caldera formation could have contributed material that was highly depleted in Ba. Plagioclase resulting from growth in a melt with such a contribution would be depleted in Ba, like those seen in the post-caldera plagioclase.

Mineral	OPX	CPX	Hornblende	Biotite	Quartz	Plagioclase	K-feldspar
Ref	*1*	*1*	*1*	*2*	*2*	*2*	*2*
Rb	0.003	0.032	0.014	3.2	0.041	0.105	1.75
Sr	0.009	0.516	0.022	0.447	-	15.633	5.4
Ba	0.003	0.131	0.044	25.533	0.022	1.515	11.45
Y	1	4	6	1.233	-	0.13	-
Ti	0.4	0.7	7	-	0.038	-	-
La	-	-	-	5.713	0.015	0.38	0.08
Ce	0.15	0.5	1.52	4.357	0.014	0.267	0.037
Pr	-	-	-	-	-	-	-
Nd	0.22	1.11	4.26	2.56	0.016	0.203	0.035
Sm	0.27	1.67	7.77	2.117	0.014	0.165	0.025
Eu	0.17	1.56	5.14	2.02	0.056	5.417	4.45

Table 5.1: Partition coefficient values for trace elements in major mineral phases present in Okataina Volcanic Center. Adapted from Rollinson (1993). Ref 1: (Table 3: Arth, 1976) Ref 2: (Tables 8-11: Nash & Crecraft, 1985)

Eruption	EM1x EM2	EM1x EM3	EM1x EM4	EM2x EM3	EM2x EM4	EM3x EM4
Pokopoko	0.737	0.016	0.222	0.549	0.151	0.525
Onuku	0.705	0.428	0.178	0.252	0.261	0.512
Rotoiti	0.374	0.629	0.21	0.233	0.219	0.251
EQF	0.554	0.2	0.125	0.444	0.4	0.185
Mangaone Unit B/C	0.447	0.526	0.122	0.394	0.387	0.637
Maketu	0.69	0.446	0.03	0.202	0.053	0.465
Hauparu xstl poor	0.622	0.668	0.066	0.05	0.157	0.626
Hauparu xstl rich	0.64	0.419	0.145	0.314	0.023	0.366
Mangaone Unit I	0.602	0.481	0.211	0.232	0.091	0.439
TeRere	0.827	0.423	0.786	0.069	0.71	0.06

Table 5.2: Correlation coefficient values calculated for mixing relationships between end-members contributions from PVA results.

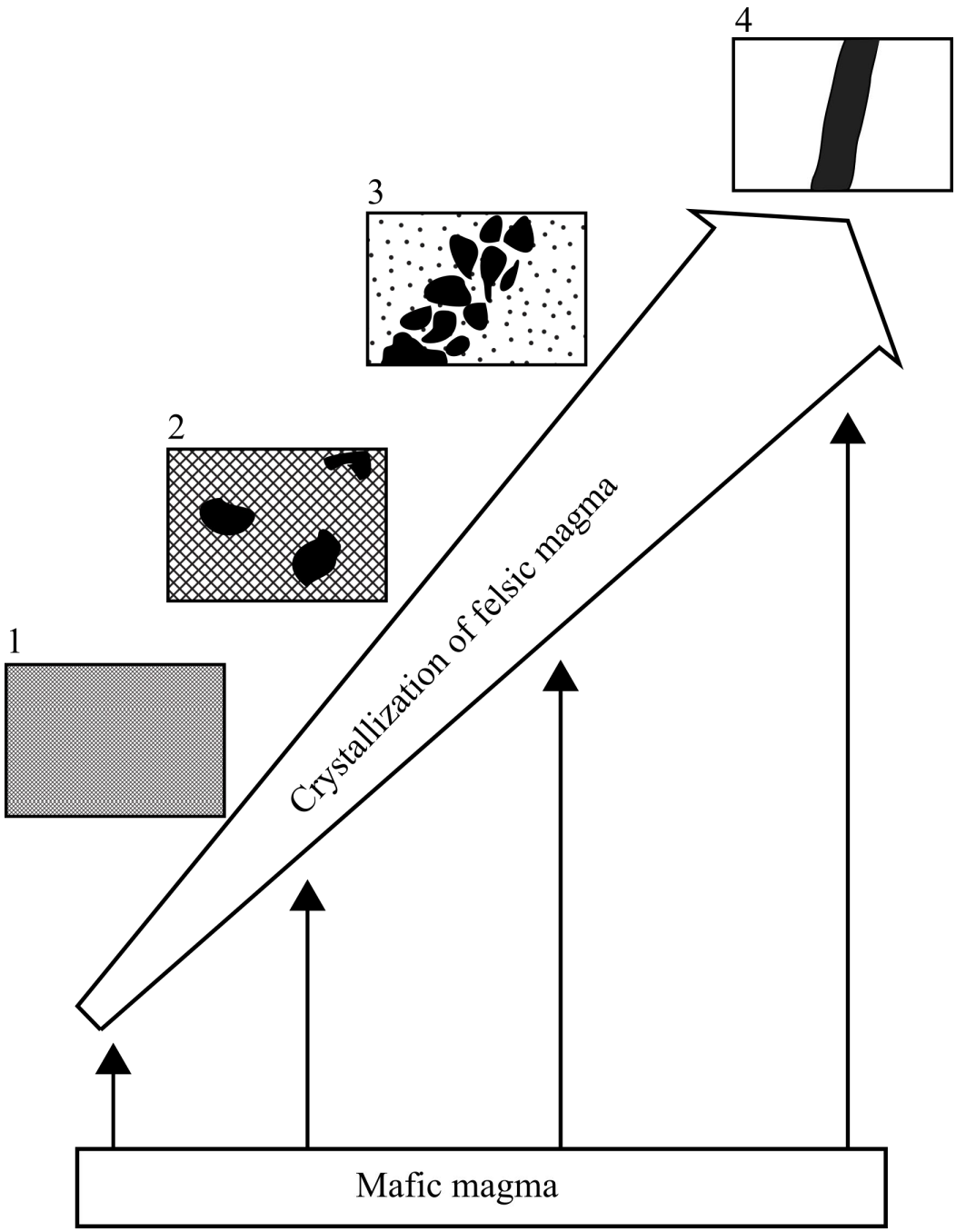

Figure 5.1: Diagram demonstrating different types of hybridization that can occur during an intrusion of mafic magma into a silicic system that is variably crystallized. 1. Mixing, 2. Mingling, 3. Filling of early fractures (composite dikes), 4. Filling of fractures (mafic dikes) Adapted from (Barbarin & Didier, 1992).

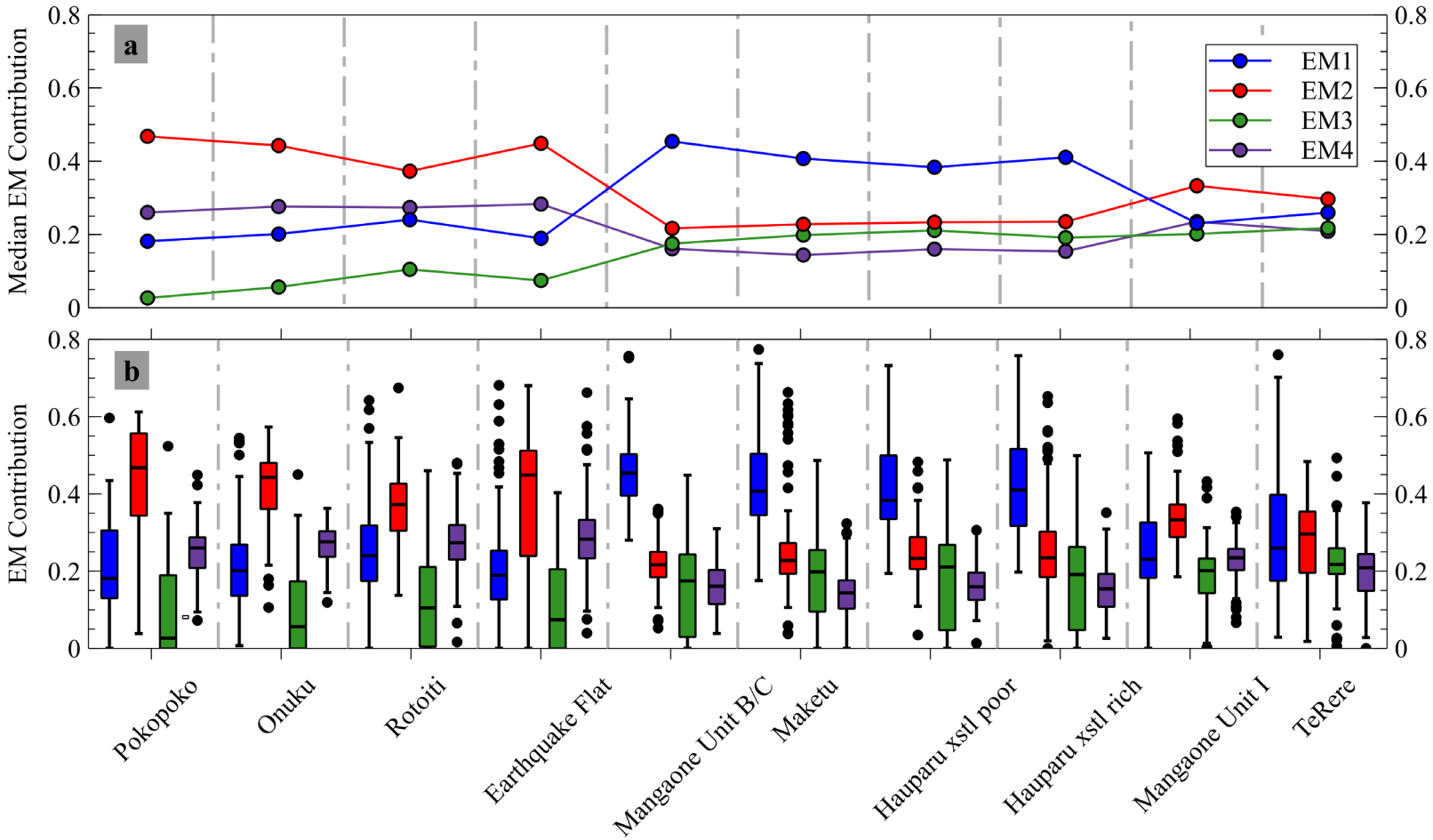

Figure 5.2 a &b: Median end-member composition for each eruption. EM contribution box plots for each eruption. Whiskers calculated using 1.5IQR method.

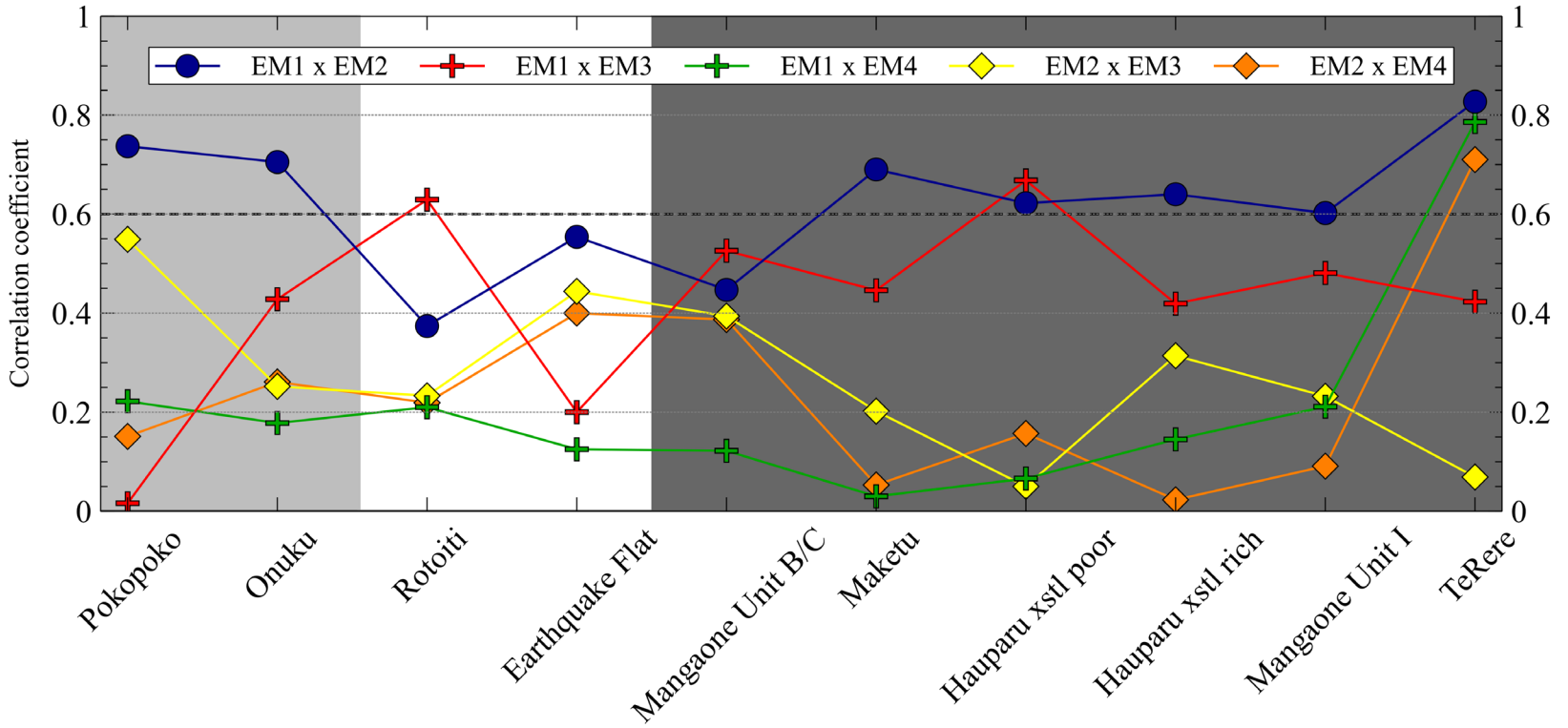

Figure 5.3: Correlation coefficient diagram for eruptions through the most recent caldera cycle at OVC. Light gray shading encompasses pre-caldera eruptions (Pokopoko and Onuku), white include syn-caldera eruptions (Rotoiti and Earthquake Flat) and dark grey represent post-caldera eruptions (Mangaone Unit B/C through TeRere

6 Conclusions

A robust assessment of the plagioclase crystals derived from the eruptions bracketing the most recent caldera forming cycle at the OVC reveals changes to the volcanic system that influenced the size and frequency of eruptions.

Our approach demonstrates that variable contributions of distinct end-members in the OVC occurred in a systemic fashion leading up to and following the Rotoiti caldera-forming eruption (Figure 6.1). We interpret the zone that contributed two distinct intermediate compositions of plagioclase to represent variations in the physical-mechanical state of the magmatic system between “cold” and “warm” storage. Periods of time characterized by a “cold” intermediate zone resulted in a high degree of mixing between the mafic and silicic end-member plagioclase reservoirs. This occurred in pre-caldera and syn-caldera eruptions. Syn-caldera plagioclase lacked a strong mixing coefficient between mafic and silicic end-members which suggests that the ability of the mafic material to ascend through the overlying melt-rich, eruptible rhyolitic magma chamber was reduced. The lack of textural heterogeneity during this time, paired with a large degree of chemical heterogeneity, points towards a magmatic system that was insulated by an extensive mush system. The mush limited mafic intrusions due to buoyancy and viscosity contrasts and provided an extensive amount of heterogeneous material to the assembling magma chamber that fed the caldera-forming eruption. Crystals that grew in this environment were texturally similar but chemically diverse. Following the rapid depressurization and evacuation of a large portion of the magmatic system, the post-caldera system was left largely frozen. Introduction of mafic magma was able to ascend through the system relatively rapidly and interact more directly with the evolved end-member reservoir. This response shows evidence of migration back towards a mushier intermediate zone by the end of the Mangaone Subgroup (textures and chemistry like those of pre / syn-caldera plagioclase).

Overall, the approach taken here, which uses textural classifications, geochemistry, and multivariate statistics has shown to be a powerful method in constraining the

interconnectedness and influence of chemical reservoirs in a system during a caldera forming sequence. Although these magmatic systems are inherently complex, and simplifying them is a delicate task, this information provides insight into what broad conditions were present during different periods of the history at OVC. In the future, investigations using different mineral populations would add different perspectives to these complex systems. Furthermore, textural analysis holds an important key to unlocking the nuance changes in volcanic systems that cannot be determined by chemical analyses alone.

Pre caldera (Pokopoko & Onuku)	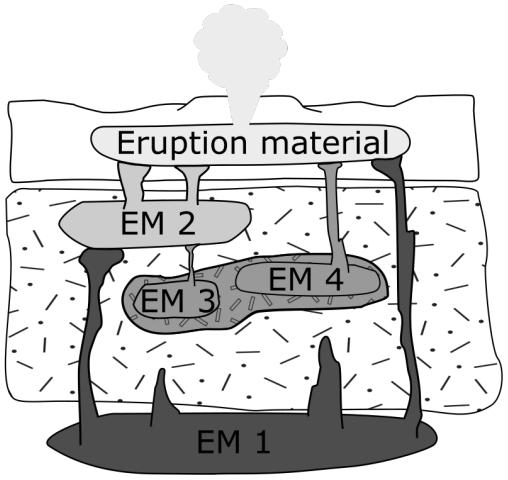
Syn caldera (Rotoiti & Earthquake Flat)	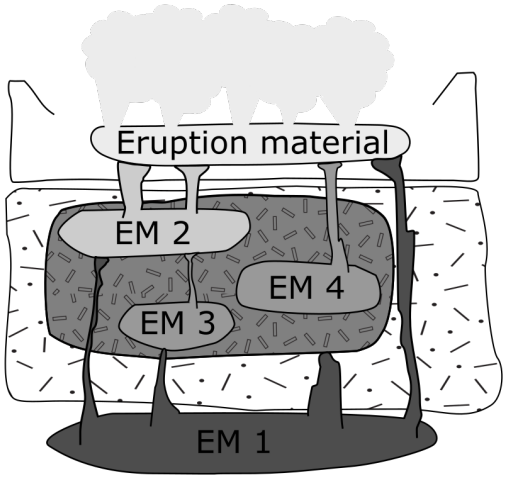
Post caldera (Mangaone Subgroup & TeRere)	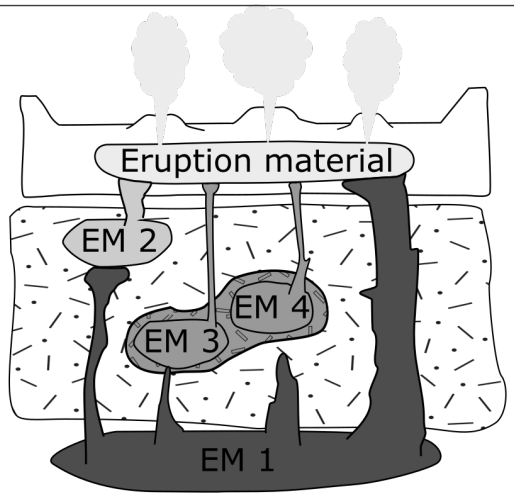

Figure 6.1 Conceptual cross section of OVC illustrating changes of thermomechanical state its during most recent caldera forming cycle. White stippled region represents crystalized rock, grey stippled indicates mush zones. Not drawn to scale.

7 References

Andersen, N. L., Singer, B. S., & Coble, M. A. (2019). Repeated Rhyolite Eruption From Heterogeneous Hot Zones Embedded Within a Cool, Shallow Magma Reservoir. *Journal of Geophysical Research: Solid Earth*, *124*(3), 2582–2600. https://doi.org/10.1029/2018JB016418

Arth, J. G. (1976). Behavior of trace elements during magmatic processes. *Journal of Research; USGS*, *4*(1), 41–47.

Bachmann, O., Deering, C. D., Ruprecht, J. S., Huber, C., Skopelitis, A., & Schnyder, C. (2011). Evolution of silicic magmas in the Kos-Nisyros volcanic center, Greece: A petrological cycle associated with caldera collapse. *Contributions to Mineralogy and Petrology*, *163*(1), 151–166. https://doi.org/10.1007/s00410-011-0663-y

Bailey, R. A., & Carr, R. G. (1994). Physical geology and eruptive history of the Matahina Ignimbrite, Taupo Volcanic Zone, North Island, New Zealand. *New Zealand Journal of Geology and Geophysics*, *37*(3), 319–344. https://doi.org/10.1080/00288306.1994.9514624

Bailey, R. A., Dalrymple, G. B., & Lanphere, M. A. (1976). Volcanism, Structure, and Geochronology of Long Valley Caldera, Mono County, California. *Jounral of Geophysical Research*, *81*(5), 725–744.

Barbarin, B., & Didier, J. (1992). Genesis and evolution of mafic microgranular enclaves through various types of interaction between coexisting felsic and mafic magmas. *Earth and Environmental Science Transactions of the Royal Society of Edinburgh*, *83*, 145–153.

Barboni, M., Boehnke, P., Schmitt, A. K., Mark Harrison, T., Shane, P., Bouvier, A. S., & Baumgartner, L. (2016). Warm storage for arc magmas. *Proceedings of the National Academy of Sciences of the United States of America*, *113*(49), 13959–13964. https://doi.org/10.1073/pnas.1616129113

Best, M. G., Christiansen, E. H., de Silva, S., & Lipman, P. W. (2016). Slab-rollback ignimbrite flareups in the southern Great Basin and other Cenozoic American arcs: A distinct style of arc volcanism. *Geosphere*, *12*(4), 1097–1135. https://doi.org/10.1130/GES01285.1

Blundy, J. D., & Shimizu, N. (1991). Trace element evidence for plagioclase recycling in calc-alkaline magmas. *Earth and Planetary Science Letters*, *102*(2), 178–197. https://doi.org/10.1016/0012-821X(91)90007-5

Brandmeier, M., & Wörner, G. (2016). Compositional variations of ignimbrite magmas in the Central Andes over the past 26 Ma — A multivariate statistical perspective.

Lithos, *262*, 713–728. https://doi.org/10.1016/j.lithos.2016.07.011

Brown, S. J. A., Burt, R. M., Cole, J. W., Krippner, S. J. P., Price, R. C., & Cartwright, I. (1998). Plutonic lithics in ignimbrites of Taupo Volcanic Zone, New Zealand; sources and conditions of crystallisation. *Chemical Geology*, *148*(1–2), 21–41. https://doi.org/10.1016/S0009-2541(98)00026-6

Candela, P. A. (1991). Physics of aqueous phase evolution in plutonic environments. *American Mineralogist*, *76*(7–8), 1081–1091.

Clark, K., Howarth, J., Litchfield, N., Cochran, U., Turnbull, J., Dowling, L., Howell, A., Berryman, K., & Wolfe, F. (2019). Geological evidence for past large earthquakes and tsunamis along the Hikurangi subduction margin, New Zealand. *Marine Geology*, *412*(March), 139–172. https://doi.org/10.1016/j.margeo.2019.03.004

Cole, J. W., Deering, C. D., Burt, R. M., Sewell, S., Shane, P. A. R., & Matthews, N. E. (2014). Okataina Volcanic Centre, Taupo Volcanic Zone, New Zealand: A review of volcanism and synchronous pluton development in an active, dominantly silicic caldera system. *Earth-Science Reviews*, *128*, 1–17. https://doi.org/10.1016/j.earscirev.2013.10.008

Cole, J. W., & Spinks, K. D. (2009). Caldera volcanism and rift structure in the Taupo Volcanic Zone, New Zealand. *Geological Society, London, Special Publications*, *327*(1), 9–29. https://doi.org/10.1144/SP327.2

Cole, J. W., Spinks, K. D., Deering, C. D., Nairn, I. A., & Leonard, G. S. (2010). Volcanic and structural evolution of the Okataina Volcanic Centre; dominantly silicic volcanism associated with the Taupo Rift, New Zealand. *Journal of Volcanology and Geothermal Research*, *190*(1–2), 123–135. https://doi.org/10.1016/j.jvolgeores.2009.08.011

Cooper, K. M., & Kent, A. J. R. (2014). Rapid remobilization of magmatic crystals kept in cold storage. *Nature*, *506*(7489), 480–483. https://doi.org/10.1038/nature12991

Danišík, M., Lowe, D. J., Schmitt, A. K., Friedrichs, B., Hogg, A. G., & Evans, N. J. (2020). Sub-millennial eruptive recurrence in the silicic Mangaone Subgroup tephra sequence, New Zealand, from Bayesian modelling of zircon double-dating and radiocarbon ages. *Quaternary Science Reviews*, *246*. https://doi.org/10.1016/j.quascirev.2020.106517

Danišík, M., Shane, P., Schmitt, A. K., Hogg, A., Santos, G. M., Storm, S., Evans, N. J., Keith Fifield, L., & Lindsay, J. M. (2012). Re-anchoring the late Pleistocene tephrochronology of New Zealand based on concordant radiocarbon ages and combined 238U/ 230Th disequilibrium and (U-Th)/He zircon ages. *Earth and Planetary Science Letters*, *349–350*, 240–250. https://doi.org/10.1016/j.epsl.2012.06.041

Deering, C. D., Bachmann, O., Dufek, J., & Gravley, D. M. (2011). Rift-relatedtransition from andesite to rhyolitevolcanism in thetaupovolcanic zone (New Zealand) controlled by crystal-melt dynamics in mush zones withvariable mineral assemblages. *Journal of Petrology*, *52*(11), 2243–2263. https://doi.org/10.1093/petrology/egr046

Deering, C. D., Cole, J. W., & Vogel, T. A. (2008). A rhyolite compositional continuum governed by lower crustal source conditions in the taupo volcanic zone, New Zealand. *Journal of Petrology*, *49*(12), 2245–2276. https://doi.org/10.1093/petrology/egn067

Deering, C. D., Cole, J. W., & Vogel, T. A. (2011). Extraction of crystal-poor rhyolite from a hornblende-bearing intermediate mush: A case study of the caldera-forming Matahina eruption, Okataina volcanic complex. *Contributions to Mineralogy and Petrology*, *161*(1), 129–151. https://doi.org/10.1007/s00410-010-0524-0

Deering, C. D., Gravley, D. M., Vogel, T. A., Cole, J. W., & Leonard, G. S. (2010). Origins of cold-wet-oxidizing to hot-dry-reducing rhyolite magma cycles and distribution in the Taupo Volcanic Zone, New Zealand. *Contributions to Mineralogy and Petrology*, *160*(4), 609–629. https://doi.org/10.1007/s00410-010-0496-0

Ewart, A. (1971). Notes on the chemistry of ferromagnesian phenocrysts from selected volcanic rocks, central volcanic region. *New Zealand Journal of Geology and Geophysics*, *14*(2), 323–340. https://doi.org/10.1080/00288306.1971.10421929

Ginibre, C., Kronz, A., & Wörner, G. (2002). High-resolution quantitative imaging of plagioclase composition using accumulated backscattered electron images: New constraints on oscillatory zoning. *Contributions to Mineralogy and Petrology*, *142*(4), 436–448. https://doi.org/10.1007/s004100100298

Ginibre, C., Wörner, G., & Kronz, A. (2002). Minor- and trace-element zoning in plagioclase: Implications for magma chamber processes at Parinacota volcano, northern Chile. *Contributions to Mineralogy and Petrology*, *143*(3), 300–315. https://doi.org/10.1007/s00410-002-0351-z

Gualda, G. A. R. (2007). Crystal and bubble populations in the early-erupted Bishop rhyolitic magma: microscopy, X-ray tomography and microanalysis of pumice clasts. *PhD Thesis, The University of Chicago*, *June*.

Houghton, B. F., Wilson, C. J. N., McWilliams, M. O., Lanphere, M. A., Weaver, S. D., Briggs, R. M., & Pringle, M. S. (1995). Chronology and dynamics of a large silicic magmatic system: central Taupo Volcanic Zone, New Zealand. *Geology*, *23*(1), 13–16. https://doi.org/10.1130/0091-7613(1995)023<0013:CADOAL>2.3.CO;2

Housh, T. B., & Luhr, J. F. (1991). Plagioclase-melt equilibria in hydrous systems. *American Mineralogist*, *76*(3–4), 477–492.

Hughes, G. R., & Mahood, G. A. (2008). Tectonic controls on the nature of large silicic calderas in volcanic arcs. *Geology*, *36*(8), 627–630. https://doi.org/10.1130/G24796A.1

Jurado-chichay, Z., & Walker, G. P. L. (2000). Stratigraphy and dispersal of the Mangaone Subgroup pyroclastic deposits , Okataina Volcanic Centre , New Zealand. *Journal of Volcanology and Geothermal Research*, *104*(1–4), 319–380.

Klemetti, E. W., Deering, C. D., Cooper, K. M., & Roeske, S. M. (2011). Magmatic perturbations in the Okataina Volcanic Complex , New Zealand at thousand-year timescales recorded in single zircon crystals. *Earth and Planetary Science Letters*, *305*(1–2), 185–194. https://doi.org/10.1016/j.epsl.2011.02.054

Lisowiec, K., Słaby, E., & Förster, H. J. (2015). Polytopic Vector Analysis (PVA) modelling of whole-rock and apatite chemistry from the Karkonosze composite pluton (Poland, Czech Republic). *Lithos*, *230*, 105–120. https://doi.org/10.1016/j.lithos.2015.05.015

Loewen, M. W. (2013). Volatile Mobility of Trace Metals in Volcanic Systems. *Oregon State University*, *Ph.D. Disseration*, 237.

Lowe, D. J., McFadgen, B. C., Higham, T. F. G., Hogg, A. G., Froggatt, P. C., & Nairn, I. A. (1998). Radiocarbon age of the Kaharoa Tephra, a key marker for late-Holocene stratigraphy and archaeology in New Zealand. *Holocene*, *8*(4), 487–495. https://doi.org/10.1191/095968398667037879

Manning, D. A. (1996). Middle-late Pleistocene tephrostratigraphy of the eastern Bay of Plenty, New Zealand. *Quaternary International*, *34*, 3–12. http://dx.doi.org/10.1016/j.cirp.2016.06.001%0Ahttp://dx.doi.org/10.1016/j.powtec.2016.12.055%0Ahttps://doi.org/10.1016/j.ijfatigue.2019.02.006%0Ahttps://doi.org/10.1016/j.matlet.2019.04.024%0Ahttps://doi.org/10.1016/j.matlet.2019.127252%0Ahttp://dx.doi.o

Marsh, B. D. (1981). On the crystallinity, probability of occurrence, and rheology of lava and magma. *Contributions to Mineralogy and Petrology*, *78*(1), 85–98. https://doi.org/10.1007/BF00371146

Melnick, D., Folguera, A., & Ramos, V. A. (2006). Structural control on arc volcanism: The Caviahue-Copahue complex, Central to Patagonian Andes transition (38°S). *Journal of South American Earth Sciences*, *22*(1–2), 66–88. https://doi.org/10.1016/j.jsames.2006.08.008

Molloy, C., Shane, P., & Nairn, I. (2008). Pre-eruption thermal rejuvenation and stirring of a partly crystalline rhyolite pluton revealed by the Earthquake Flat Pyroclastics deposits, New Zealand. *Journal of the Geological Society*, *165*(1), 435–447. https://doi.org/10.1144/0016-76492007-071

Nairn, I. A. (2002). Geology of the Okataina Volcanic Centre. *Institute of Geological and Nuclear Sciences*, *Geological*, 156.

Nairn, I. A., & Cole, J. W. (1981). Basalt dikes in the 1886 tarawera rift. *New Zealand Journal of Geology and Geophysics*, *24*(5–6), 585–592. https://doi.org/10.1080/00288306.1981.10421534

Nakamura, M., & Shimakita, S. (1998). Dissolution origin and syn-entrapment compositional change of melt inclusion in plagioclase. *Earth and Planetary Science Letters*, *161*(1–4), 119–133. https://doi.org/10.1016/S0012-821X(98)00144-7

Nash, W. P., & Crecraft, H. R. (1985). Partition coefficients for trace elements in silicic magmas. *Geochimica et Cosmochimica Acta*, *49*(11), 2309–2322. https://doi.org/10.1016/0016-7037(85)90231-5

Nixon, G. T., & Pearce, T. H. (1987). Laser-interferometry study of oscillatory zoning in plagioclase : The record of magma mixing and phenocryst recycling in calc-alkaline magma chambers , Iztaccihuatl volcano , Mexico. *American Mineralogist*, *72*(11), 1144–1162.

Pearce, T. H., & Kolisnik, A. M. (1990). Observations of plagioclase zoning using interference imaging. *Earth-Science Reviews*, *29*, 9–26.

Pearce, T. H., Russell, J. K., & Wolfson, I. (1987). Laser-interference and Nomarski interference imaging of zoning profiles in plagioclase phenocrysts from the May 18, 1980, eruption of Mount St. Helens, Washington. *American Mineralogist*, *72*(11–12), 1131–1143.

Pitcher, B. W., & Kent, A. J. R. (2019). Statistics and segmentation: Using Big Data to assess Cascades arc compositional variability. *Geochimica et Cosmochimica Acta*, *265*, 443–467. https://doi.org/10.1016/j.gca.2019.08.035

Rooney, T. O., & Deering, C. D. (2014). Conditions of melt generation beneath the Taupo Volcanic Zone: The infl uence of heterogeneous mantle inputs on large-volume silicic systems. *Geology*, *42*(1), 3–6. https://doi.org/10.1130/G34868.1

Rubin, A., Cooper, K. M., Leever, M., Wimpenny, J., Deering, C., Rooney, T., Gravley, D., & Yin, Q. zhu. (2016). Changes in magma storage conditions following caldera collapse at Okataina Volcanic Center, New Zealand. *Contributions to Mineralogy and Petrology*, *171*(1), 1–18. https://doi.org/10.1007/s00410-015-1216-6

Rubin, A. E., Cooper, K. M., Till, C. B., Kent, A. J. R., Costa, F., Bose, M., Gravley, D., Deering, C., & Cole, J. (2017). Rapid cooling and cold storage in a silicic magma reservoir recorded in individual crystals. *Science*, *356*(June), 1154–1156. https://doi.org/10.1126/science.aam8720

Ruprecht, P., & Wörner, G. (2007). Variable regimes in magma systems documented in plagioclase zoning patterns: El Misti stratovolcano and Andahua monogenetic cones. *Journal of Volcanology and Geothermal Research*, *165*(3–4), 142–162. https://doi.org/10.1016/j.jvolgeores.2007.06.002

Sas, M. (2020). Isotopic and geochemical records of magmatic processes captured in crystals from rhyolites at Okataina volcano. *University of Aukland*, 172.

Sawyer, D. A., Fleck, R. J., Lanphere, M. A., Warren, R. G., Broxton, D. E., & Hudson, M. R. (1994). Episodic caldera volcanism in the Miocene southwestern Nevada volcanic field: revised stratigraphic framework, 40Ar/39Ar geochronology, and implications for magmatism and extension. *Geological Society of America Bulletin*, *106*(10), 1304–1318. https://doi.org/10.1130/0016-7606(1994)106<1304:ecvitm>2.3.co;2

Schmitz, M. D., & Smith, I. E. M. (2004). The petrology of the Rotoiti eruption sequence, Taupo Volcanic zone: An example of fractionation and mixing in a rhyolitic system. *Journal of Petrology*, *45*(10), 2045–2066. https://doi.org/10.1093/petrology/egh047

Shane, P. (2015). Contrasting plagioclase textures and geochemistry in response to magma dynamics in an intra-caldera rhyolite system, Okataina volcano. *Journal of Volcanology and Geothermal Research*, *297*, 1–10. https://doi.org/10.1016/j.jvolgeores.2015.03.013

Skirius, C. M., Peterson, J. W., & Anderson, A. T. (1990). Homogenizing rhyolitic glass inclusions from the Bishop Tuff. *American Mineralogist*, *75*(11–12), 1381–1398. https://doi.org/10.1016/j.clinbiochem.2007.01.023

Słaby, E., De Campos, C. P., Majzner, K., Simon, K., Gros, K., Moszumańska, I., & Jokubauskas, P. (2017). Feldspar megacrysts from the Santa Angélica composite pluton — Formation/transformation path revealed by combined CL, Raman and LA-ICP-MS data. *Lithos*, *277*, 269–283. https://doi.org/10.1016/j.lithos.2016.09.016

Smith, V. C., Shane, P., & Nairn, I. A. (2005). Trends in rhyolite geochemistry, mineralogy, and magma storage during the last 50 kyr at Okataina and Taupo volcanic centres, Taupo Volcanic Zone, New Zealand. *Journal of Volcanology and Geothermal Research*, *148*(3–4), 372–406. https://doi.org/10.1016/j.jvolgeores.2005.05.005

Smith, V. C., Shane, P., Smith, I. E. M., Smith, V. C., & Shane, P. (2002). Tephrostratigraphy and geochemical fingerprinting of the Mangaone Subgroup tephra beds , Okataina Volcanic Centre , New Zealand. *New Zealand Journal of Geology and Geophysics*, *45*, 207–219. https://doi.org/10.1080/00288306.2002.9514969

Smith, V., Shane, P., & Nairn, I. (2010). Insights into silicic melt generation using plagioclase, quartz and melt inclusions from the caldera-forming Rotoiti eruption, Taupo volcanic zone, New Zealand. *Contributions to Mineralogy and Petrology*, *160*(6), 951–971. https://doi.org/10.1007/s00410-010-0516-0

Spinks, K. D., Acocella, V., Cole, J. W., & Bassett, K. N. (2005). Structural control of volcanism and caldera development in the transtensional Taupo Volcanic Zone, New Zealand. *Journal of Volcanology and Geothermal Research*, *144*(1-4 SPEC. ISS.), 7–22. https://doi.org/10.1016/j.jvolgeores.2004.11.014

Streck, M. J. (2008). Mineral textures and zoning as evidence for open system processes. *Reviews in Mineralogy and Geochemistry*, *69*(1983), 595–622. https://doi.org/10.2138/rmg.2008.69.15

Szymanski, D. W., Patino, L. C., Vogel, T. A., & Alvarado, G. E. (2013). Evaluating complex magma mixing via polytopic vector analysis (PVA) in the papagayo tuff, Northern Costa Rica: Processes that form continental crust. *Geosciences (Switzerland)*, *3*(3), 585–615. https://doi.org/10.3390/geosciences3030585

Tefend, K. S., Vogel, T. A., Flood, T. P., & Ehrlich, R. (2007). Identifying relationships among silicic magma batches by polytopic vector analysis: A study of the Topopah Spring and Pah Canyon ash-flow sheets of the southwest Nevada volcanic field. *Journal of Volcanology and Geothermal Research*, *167*(1–4), 198–211. https://doi.org/10.1016/j.jvolgeores.2006.07.011

Tepley, F. J., Davidson, J. P., & Clynne, M. A. (1999). Magmatic interactions as recorded in plagioclase phenocrysts of Chaos Crags, Lassen Volcanic Center, California. *Journal of Petrology*, *40*(5), 787–806. https://doi.org/10.1093/petroj/40.5.787

Tsuchiyama, A. (1985). Contributions to Mineralogy and Dissolution kinetics of plagioclase in the melt of the system diopside-albite-anorthite , and origin of dusty plagioclase in andesites. *Contributions to Mineralogy and Petrology*, *89*(1), 1–16.

Viccaro, M., Giacomoni, P. P., Ferlito, C., & Cristofolini, R. (2009). Tracking magma dynamics at Mount Etna from plagioclase textures and compositional zoning Lithos Dynamics of magma supply at Mt . Etna volcano (Southern Italy) as revealed by textural and compositional features of plagioclase phenocrysts. *LITHOS*, *116*(1–2), 77–91. https://doi.org/10.1016/j.lithos.2009.12.012

Vogel, T. A., Hidalgo, P. J., Patino, L., Tefend, K. S., & Ehrlich, R. (2008). Evaluation of magma mixing and fractional crystallization using whole-rock chemical analyses: Polytopic vector analyses. *Geochemistry, Geophysics, Geosystems*, *9*(4), 1–27. https://doi.org/10.1029/2007GC001790

Wilson, C. J. N., Houghton, B. F., McWilliams, M. O., Lanphere, M. A., Weaver, S. D., & Briggs, R. M. (1995). Volcanic and structural evolution of Taupo Volcanic Zone,

New Zealand: a review. *Journal of Volcanology and Geothermal Research*, *68*(1–3), 1–28. https://doi.org/10.1016/0377-0273(95)00006-G

Wilson, C. J. N., Rogan, A. M., Smith, I. E. M., Northey, D. J., Nairn, I. A., & Houghton, B. F. (1984). Caldera volcanoes of the Taupo volcanic zone, New Zealand. *Journal of Geophysical Research*, *89*(B10), 8463–8484. https://doi.org/10.1029/JB089iB10p08463

Wolff, J. A., Ellis, B. S., Ramos, F. C., Starkel, W. A., Boroughs, S., Olin, P. H., & Bachmann, O. (2015). Remelting of cumulates as a process for producing chemical zoning in silicic tuffs: A comparison of cool, wet and hot, dry rhyolitic magma systems. *Lithos*, *236–237*, 275–286. https://doi.org/10.1016/j.lithos.2015.09.002